AFRL-RD-PS-
TR-2017-0046

BEAM REQUIREMENTS FOR A TWO-STREAM INSTABILITY AMPLIFIER

Peter Mardahl and
Michael Lambrecht

23 June 2017

Final Report

AIR FORCE RESEARCH LABORATORY
Directed Energy Directorate
3550 Aberdeen Ave SE
AIR FORCE MATERIEL COMMAND
KIRTLAND AIR FORCE BASE, NM 87117-5776

NOTICE AND SIGNATURE PAGE

Using Government drawings, specifications, or other data included in this document for any purpose other than Government procurement does not in any way obligate the U.S. Government. The fact that the Government formulated or supplied the drawings, specifications, or other data does not license the holder or any other person or corporation; or convey any rights or permission to manufacture, use, or sell any patented invention that may relate to them.

Qualified requestors may obtain copies of this report from the Defense Technical Information Center (DTIC) (http://www.dtic.mil).

AFRL-RD-PS-TR-2017-0046 HAS BEEN REVIEWED AND IS APPROVED FOR PUBLICATION IN ACCORDANCE WITH ASSIGNED DISTRIBUTION STATEMENT.

//PETER MARDAHL//	//ANDREW GREENWOOD//
PETER MARDAHL, DR-IV	ANDREW GREENWOOD, DR-IV
Project Officer	Branch Chief, Modeling and Effects

This report is published in the interest of scientific and technical information exchange, and its publication does not constitute the Government's approval or disapproval of its ideas or findings.

REPORT DOCUMENTATION PAGE

Form Approved
OMB No. 0704-0188

1. REPORT DATE *(DD-MM-YYYY)*	**2. REPORT TYPE**	**3. DATES COVERED** *(From - To)*
23-06-2017	Final Report	10-01-2012 – 09-30-2016

4. TITLE AND SUBTITLE

Beam Requirements for a Two-Stream Instability Amplifier

5a. CONTRACT NUMBER
In-House

5b. GRANT NUMBER

5c. PROGRAM ELEMENT NUMBER

6. AUTHOR(S)

Peter Mardahl and Michael Lambrecht

5d. PROJECT NUMBER

5e. TASK NUMBER
DF702172

5f. WORK UNIT NUMBER
D01K

7. PERFORMING ORGANIZATION NAME(S) AND ADDRESS(ES)

Air Force Research Laboratory
3550 Aberdeen Avenue SE
Kirtland AFB, NM 87117-5776

8. PERFORMING ORGANIZATION REPORT NUMBER

9. SPONSORING / MONITORING AGENCY NAME(S) AND ADDRESS(ES)

Air Force Research Laboratory
3550 Aberdeen Avenue SE
Kirtland AFB, NM 87117-5776

10. SPONSOR/MONITOR'S ACRONYM(S)
AFRL/RDHE

11. SPONSOR/MONITOR'S REPORT NUMBER(S)
AFRL-RD-PS-TR-2017-0046

12. DISTRIBUTION / AVAILABILITY STATEMENT

Approved for public release, distribution is unlimited.

13. SUPPLEMENTARY NOTES

RDMX-17-14634 22March2018. AFMC-2018-0377 13 September 2018. "Government Purpose Rights"

14. ABSTRACT

Theoretical and simulation work has raised the possibility of a GW-class two-stream instability based amplifier using two co-propagating relativistic beams of different currents and energies that achieves high efficiency (50%). With some selected beam parameters, we have achieved simulated signal gains in excess of 35dB in the squared amplitude of beam modulation ~I2, which is proportional to the maximum RF power that could be extracted. We have investigated the effect of beam temperature and annular beam thickness on the performance of this device. Beam energy spread has to be kept very low (< 1% of the beam energy) to achieve high levels of bunching in the beams, failure to do so can result in > 75% loss in magnitude of ~Imax. Also, the thickness of the annular beams used has to be tightly constrained, or similar performance degradation results. Beam energy spread is shown to influence the maximum achievable bunching prior to saturation, while not modifying growth rate. These beam energy spread constraints combined with the requirement to produce very high current (multi-kA), very small radius (< 2cm), very small thickness (<= 1mm) beams makes practical realization of a 100MW+ amplifier based on relativistic two-stream instability challenging. Attempts to relax these constraints by moving from a 9GHz amplifier to a larger 3GHz amplifier have resulted in performance degradation while still posing a presently insurmountable problem for the electron beam gun designer.

15. SUBJECT TERMS

GW-class amplifier; high power microwave; two-stream instability

16. SECURITY CLASSIFICATION OF:			**17. LIMITATION OF ABSTRACT**	**18. NUMBER OF PAGES**	**19a. NAME OF RESPONSIBLE PERSON**
a. REPORT	**b. ABSTRACT**	**c. THIS PAGE**			Peter Mardahl
UNCLASSIFIED	UNCLASSIFIED	UNCLASSIFIED	SAR	68	**19b. TELEPHONE NUMBER** *(include area code)*

This page intentionally left blank.

TABLE OF CONTENTS

List of Figures

Figure **Page**

List of Tables

Table **Page**

This page intentionally left blank.

1.0 SUMMARY

The relativistic two stream amplifier promised to be a gigawatt-class broadband device capable in principle of greater than 20-dB amplification of an input signal across octaves of bandwidth. Implementation of a design that meets this performance seems to be impractical given current technology. The issue is that providing two high current (kA-class) annular electron beams with hundreds of kV of energy, millimeters thick and also separated by millimeters, with both beams having very low spread in velocities cannot be done in practice with any known technique. Simulations showed that anything more than 1% of beam energy spread drastically reduced performance to the point of being largely uninteresting. Attempted gun designs yielded beam spreads that were either too high or that failed to provide the current/voltage required. The simulations (and theory) did show that significant signal amplification was possible to obtain if low beam spread and the requisite beam geometry, currents, and voltages were provided–a simple matter in simulation, presently unachievable experimentally. Because of the unfavorable gun design results and the determination via simulation that currently available electron gun technologies would never meet the requirements, experimental realization of the device was never attempted and funding reserved for experimental efforts was applied to other Air Force Office of Scientific Research (AFOSR) projects. Future advancements in cathode and electron gun technology may eventually allow these issues to be surmounted.

2.0 INTRODUCTION

Theoretical and simulation work has raised the possibility of a gigawatt (GW) class two-stream instability based amplifier using two co-propagating relativistic beams of different currents and energies that achieves high efficiency (50%) [1]. With some selected beam parameters, we have achieved simulated signal gains in excess of 35dB in the squared amplitude of beam modulation $\tilde{I}^2$, which is proportional to the maximum radio frequency (RF) power that could be extracted. We have investigated the effect of beam temperature and annular beam thickness on the performance of this device. Beam energy spread has to be kept very low ($<$ 1% of the beam energy) to achieve high levels of bunching in the beams, failure to do so can result in $>$75% loss in magnitude of $\tilde{I}_{max}$. Also, the thickness of the annular beams used has to be tightly constrained, or similar performance degradation results. Beam energy spread is shown to influence the maximum achievable bunching prior to saturation, while not modifying growth rate. These beam energy spread constraints combined with the requirement to produce very high current (multi-kA), very small radius ($<$2cm), very small thickness ($<=$ 1mm) beams makes practical realization of a 100MW+ amplifier based on relativistic two-stream instability challenging. Attempts to relax these constraints by moving from a 9GHz amplifier to a larger 3GHz amplifier have resulted in performance degradation while still posing a presently insurmountable problem for the electron beam gun designer.

The concept of the two-stream amplifier is to exploit the well-known two-stream plasma instability to construct an amplifier. This instability is an absolute instability, which would ordinarily preclude use for amplification. However, when two co-propagating beams of different energies interact, the instability propagates with the beams and becomes convective in the frame of the amplifier device, as shown in Figure 1.

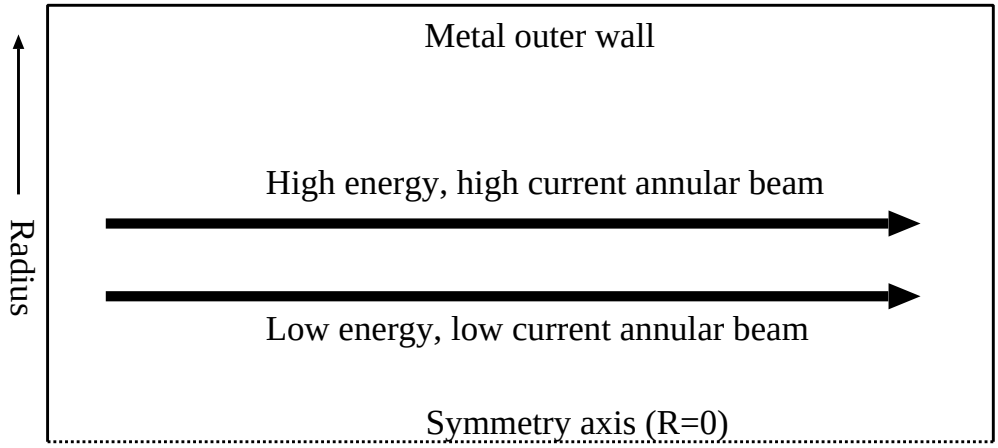

Figure 1: With Co-Propagating Beams, the Two-Stream Absolute Instability Becomes Convective

Two-stream instability amplifiers were first examined shortly after World War II [2, 3]. The amplifiers produced used lower energy beams than in this work and in the more recent work [1] which employ relativistic beams. The World War II era results were considered inferior to helical traveling wave-tube (TWT) amplifiers: the two-stream instability, while capable of bunching beams, does not directly produce RF but must be interacted with an RF or microwave circuit. The broadband circuit used for RF extraction was a helical structure, and the resulting two-stream amplifiers were inferior in efficiency and complexity to standard helix TWTs [4]. A key issue identified with the two stream amplifiers of the time was that the beam temperature was too high for efficient operation.

More recent theory and simulation work examined the case of relativistic beams for two-stream amplifiers and derived results indicating the possibility of efficiencies approaching 50% [1]. This work proposed a klystron-like extraction technique (described as the Relativistic Two-Stream Klystron Amplifier (RTKA)), and their notional device design is shown in Figure 2. This work was extended with the publication of a simulated higher frequency, higher power concept [5], the Relativistic Two-Stream Amplifier (RTSA) which exhibited gains of 30dB per meter in simulation, in agreement with the theory. This work proposed a klystron-like resonant cavity extraction mechanism for converting the beam modulation into RF radiation, but didn't actually simulate this conversion.

There are several potential advantages to the two-stream approach to RF amplification. First is that the two-stream instability's growth rate, as shown in Figure 3, is very broadband, opening the possibility of a 100MW+ amplifier of unprecedented bandwidth. Here, one beam had a beam voltage of 210kV, a beam current of 83A, and a beam radius of .513cm. The second beam had a beam voltage of 450kV, a beam current of 3kA, and a

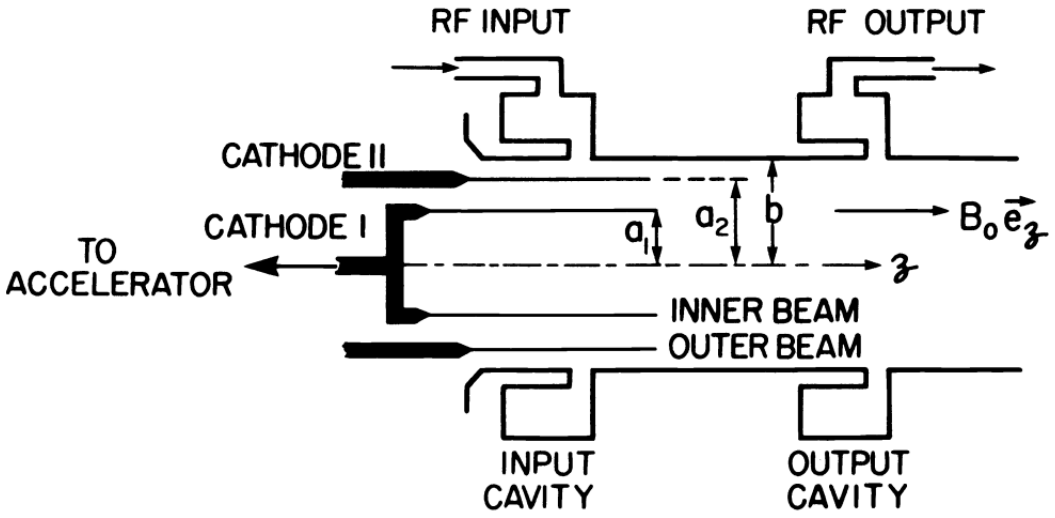

Figure 2: Notional Two-Stream Klystron From Chen et. al.

beam radius of .65cm. The beam tunnel radius was .95cm. The theory used by the references does not include beam energy spread (beam temperature). Second, the interaction between the beams does not require a co-propagating electromagnetic mode. Therefore, the two beams can be interacted in a beam tunnel that is cut-off for the frequencies to be amplified. This is a considerable advantage given that one of the largest difficulties with any amplifier is preventing the amplifier from oscillating. Since the frequency to be amplified can be cut-off in the beam interaction region for the transverse magnetic (TM_{01}) mode, that prevents it from being reflected off of the extraction mechanism, returning to the origin of the beam, and re-seeding itself. Thus, choice of the beam parameters and cut-off frequency can be used to effectively suppress oscillation. Third is the prospect of high power. Since high current relativistic beams are used, RF powers in excess of 100MW seemed achievable.

Obvious disadvantages include the requirement to produce and interact two relativistic beams of significantly different energies in close proximity, and the problem of how to efficiently extract energy from the modulated beam. The klystron-like output concept proposed in [5] seems quite viable since it works for klystrons, however, a resonant cavity extractor is necessarily going to be fairly narrowband. Also, the post World War II attempts at producing viable two-stream amplifiers showed that control of the beam temperature is a key issue.

Our work begins with a reproduction of results similar to [5]. We were unable to exactly reproduce the work because key simulation parameters, such as input and exit boundary conditions, time step and computational cell size, and any filtering techniques used were not given in the reference or otherwise made available by the authors. Nevertheless, with considerable effort, we were able to reproduce a reasonably good match to the previously published results, and move on to the study of nonidealities such as beam energy spread and beams larger in annular size than ideal. Section 3.0 describes the geometry,

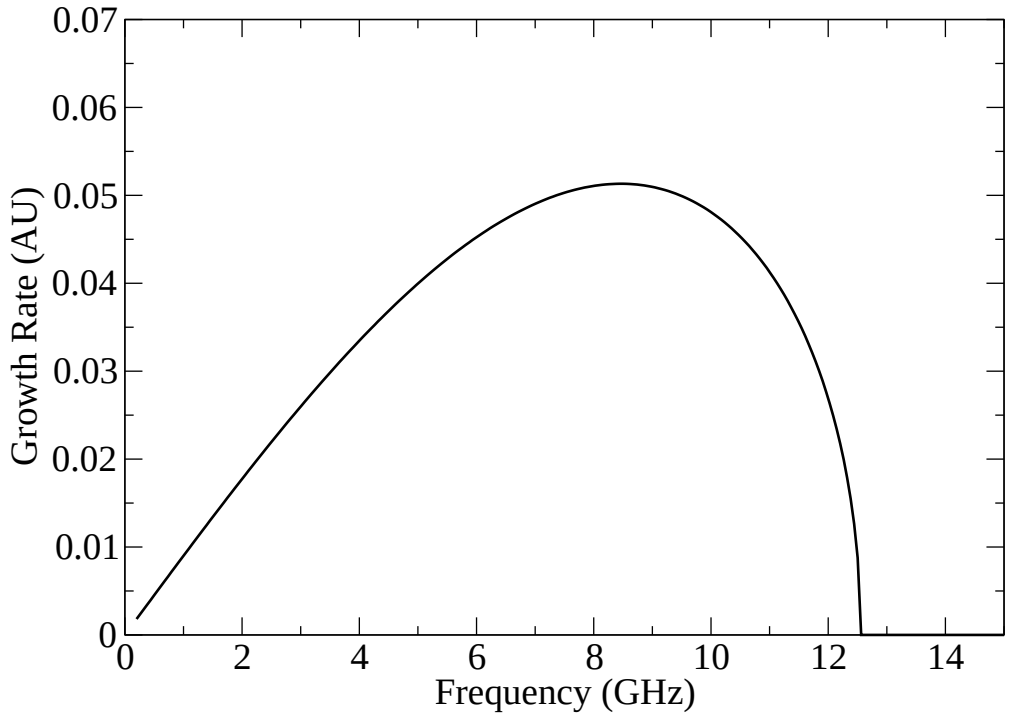

Figure 3: Example Theory Curve for a Two-Stream Instability on Co-Propagating Beams

numerical parameters, boundary conditions, analysis techniques, and filtering methods that we used, and shows our initial beam parameter designs for 3.375GHz, 11.4GHz, and 9GHz versions of the two stream amplifiers. Section 4.0 gives some theoretical predictions of growth rates based on linear theory, and shows we were able to reproduce results from [5]. Also in Section 4.0 we show the deleterious effects on amplification if non-ideal beam parameters are used, namely adding beam energy spread and using beams with annular thickness $>$ 1mm. Finally in Section 5.0 we present our conclusions and delineate required future work to achieve a practical 100MW+ amplifier based on two-stream instability.

3.0 METHODS, ASSUMPTIONS, AND PROCEDURES

3.1 Numerical Simulation Methods and Parameters

Simulations were performed with Improved Concurrent Electromagnetic Particle in Cell code (ICEPIC) [6], a relativistic electromagnetic particle-in-cell code. Some simulations were also performed using the Object Oriented Particle in Cell (XOOPIC) [7] code as well, but these were done only to confirm the presence of numerical Cerenkov radiation as a check on the ICEPIC simulations, we will not present XOOPIC results here, merely state that numerical noise properties and Cerenkov radiation effects were comparable.

For all simulations, a spatially uniform .6 Tesla axial magnetic field was applied to confine the electron beams. Simulations were generally performed in two dimensions, using

r-z geometry (this assumes azimuthal symmetry about the z axis), occasionally three dimensional (3D) simulations were performed. Two concentric annular beams of varying thicknesses, direct current (DC) currents, energies, and temperatures were introduced into the simulation regime. An input signal was introduced into the simulation by imposing a sinusoidal time variation in the current of the outer beam as it was launched. This outer beam was generally more energetic and had a larger DC current than the inner beam.

The two annular electron beams were launched from a perfectly conducting metal surface in the +z direction, with varying beam currents, energies, temperatures and radial annular thicknesses, though typically the latter is 1mm unless otherwise noted. Beam energy was not ramped: beam current was ramped up linearly over 10ns from 0 to the desired value.

Various geometries were used, however, since we eventually became interested in studying a worst-case scenario where self-oscillations could occur and dominate the physics, we eventually arrived at the use of a simple hollow cylindrical cavity geometry for most simulations. This cylinder was bounded on top, bottom and side with perfect metal conductor. Any electromagnetic mode would therefore have no means of escaping except via interaction with the beams, and conditions would be ideal for parasitic oscillations due to electromagnetic modes to occur. The reasoning was that if parasitic oscillations did not occur despite ideal conditions for them to exist, then the design was inherently resistant to parasitic oscillations.

In order to study modulation amplification due to beam interaction, the current was measured periodically in z by measuring the magnetic field outside the maximum beam radius, and applying Ampere's law, $I_{enclosed}=\oint B \cdot dl$. This method of measuring current supplied a fair amount of filtering of high frequency noise associated with the discreteness of particles. Direct measurement of either the current density on the mesh (Jz), or the particle flux, produced unsatisfactorily noisy results. The current signals were then frequency-analyzed via Fourier transform and the amplitudes of the signals measured. Signal gain was determined by comparing the peak amplitude of current modulation $\tilde{I}$ reached to the initial signal amplitude measured just inside the input.

The energetic beams in this simulation were highly susceptible to numerical Cerenkov radiation. This is a numerical effect in finite difference time domain (FDTD) particle in cell (PIC) simulations where wavelengths that are short compared to the computational mesh size (i.e., waves that are poorly resolved by the computational mesh) propagate at speeds slower than physical. This allows the simulated beam, generally propagating at spreads near to c, the speed of light, to have non-physical interactions with the slowed-down short wavelength radiation and results in short-wavelength numerical (non-physical) Cerenkov radiation. Since this interaction is nonphysical and has deleterious effects upon beam temperature, Friedman filtering [8] was applied with θ=0.2 to attenuate short wavelength electromagnetic (EM) waves. Per the reference [8], this level of filtering provides a negligible attenuation (approximately 10^{-4} attenuation rate per m vs. approx. .06 per cm analytically expected instability growth, a factor of 60,000) of wavelengths in the 1-12GHz range, the range of frequencies we were interested in amplifying, and also approximately the range of frequencies that theory predicts would be amplified via the two-stream mechanism. Attenuation at higher frequencies was much higher–the attenuation number provided for 1-12GHz was provided to demonstrate the negligible impact of

filtering on the physics of interest.

To provide even more filtering, when Fourier analysis of the beam modulation amplitude was performed, frequencies higher than 30GHz were excluded. Signals at these frequencies are generally the result of particle discreteness or "shot noise". In a PIC simulation shot noise will be much larger than experiment, since PIC particles are weighted from 10^7 to 10^9 times as much as a real electron. (Computer resources that can model 10^9 more particles than were modeled are too expensive). This implies a nonphysical increase in particle noise of the square-root of that factor, or approximately 10^4. Particle noise was also limited by emitting 100 particles per emitting cell per time step instead of 1 particle per time step as is often done. (Particle emission within a given cell was evenly distributed in time during a time step and randomly distributed over the face of the cell.)

Notably, it required all four methods of reducing numerical issues (emitting 100 or more particles per cell per time step, application of Friedman filter to remove numerical Cerenkov radiation, application of low-pass filter to results, and using the magnetic field and Ampere's law to measure current), to produce current modulation results that were sufficiently clear of noise to enable automatic detection of the seed and amplified signals. We believe that any PIC code using the standard FDTD Yee PIC algorithms would require the same measures to achieve good results, based upon how they work, and indeed XOOPIC [7] simulations exhibited all the same numerical issues seen in the ICEPIC simulations.

Table 1 shows the baseline geometry and numerical parameters for the designs examined. When discussing results, we will identify when we have departed from using these baseline parameters. Initial work focused on the 11.4GHz design, but in an attempt to relax the geometric constraints on the electron beams, we also attempted a 3.375GHz design. In the table, dz is the numerical mesh spacing in the z direction (the direction of electron beam propagation), dr is the numerical mesh spacing in the radial direction (transverse to electron beam propagation), % of Courant is the percentage of the maximum size time step for which the code would be stable given the use of the Yee algorithm and the mesh size, θ is the Friedman filter parameter, and B is the magnetic field. It is notable that best results with the Yee algorithm occur with % of Courant as close to 100 as possible, for example, 99%. However, when combined with the Friedman filtering, numerical stability requires a lower fraction of Courant be used, we found 90% of Courant to be stable.

Table 2 shows the baseline beam parameters for the designs. These were frequently varied to discover optimum points of operation and to discover the effect of non-ideal circumstances, particular beams radially wider than desired and also beam energy spread. I_{bi} is the inner beam current, V_{bi} is the inner beam energy, R_{bi} is the inner beam radius,t_{bi}

Table 1: Physical and Numerical Baseline Parameters

Design	Drift tube length	Drift tube radius	dz	dr	% of Courant	θ	B
3.375GHz	2.264m	2.54cm	.5mm	.5mm	90	.2	.6
11.4GHz	.765m	.95cm	.5mm	.5mm	90	.2	.6
9GHz	2.264m	.95cm	.5mm	.5mm	90	.2	.6

Table 2: Baseline Electron Beam Parameters

Design	I_{bi}	V_{bi}	R_{bi}	t_{bi}	I_{bo}	V_{bo}	R_{bo}	t_{bo}
3.375GHz	1kA	220kV	2.08cm	1mm	5kA	400kV	2.29cm	1mm
11.4GHz	.36kA	240kV	.3cm	1mm	1.2kA	550kV	.2cm	1mm
9GHz	1kA	220kV	2.08cm	1mm	5kA	400kV	2.25cm	1mm

is the inner beam's annular thickness. The beam parameters for the outer beam are analogously I_{bo}, V_{bo}, R_{bo}, and t_{bo}.

The beams were launched from metal at the left hand side of the simulation, at the specified energies. Beam depression, the space charge of the beam itself, results in the beam being decelerated from its initial (launch) energy. Thus, the resulting beam energy in the center of the device is somewhat lower than the beam insertion energy, and due to nonlinear effects, the resulting beam energies can be hard to predict. For very compact, high current beams that are far from conducting walls, this can be very significant. For simplicity, and because input beam voltage is the parameter easily controlled by experimentalists, we describe simulations in terms of the input beam parameters and not in terms of the beam energies that result after beam depression has modified the beam. Theoretical calculations however depend upon the resulting beam energy. We have taken the approach of using theory for guidance and using groups of relatively inexpensive two-dimensional (2D) simulations to scan beam energies to find optimal operation, which we considered to be maximum gain in the quantity $\tilde{I}$, the modulation in beam current. Beam energy spread was added by means of using the "temp" feature of ICEPIC, which adds a temperature in the form of a Maxwellian distribution to the beam. A 1% beam spread of a 500keV beam was modeled by setting the "temp" variable to 5keV, for example.

In this work, we will often report amplification results as a 'heat map', which shows two beam parameters on the X and Y axes (often $V_{bi}$and V_{bo}), and display the modulation fraction $|\tilde{I}|/I_{total}$ as a color. The modulation fraction reported is the maximum modulation fraction measured along the length of the device. For example, if the modulation fraction peaks at .15 at a distance of 60cm, but then drops thereafter, the heat map will report a modulation fraction of .15. The modulation fraction was measured via Fourier transform of the current waveform and the peak frequency's magnitude value extracted. We report in this way because if peak power is desired, one is free to shorten the device to the length at which modulation fraction is maximized. Figure 11, for example, is reported in this way.

An example ICEPIC input file, in the ".in" format that requires preprocessing, is given in APPENDIX A.

3.2 Growth Rate Theory

Theory computations were computed from the dispersion relation,

$$1 - \sum_{\alpha=1}^{2} \frac{\epsilon_\alpha (c^2 k_z^2 - \omega^2)}{(\omega - k_z V_\alpha)^2} + \frac{ln(a_2/a_1)}{ln(b/a_1)} \frac{\epsilon_1 \epsilon_2 (c^2 k_z^2 - \omega^2)^2}{(\omega - k_z V_1)^2 (\omega - k_z V_2)^2} = 0 \tag{1}$$

where c is the speed of light, k_z is the wave number in the z direction, ω is the angular frequency of the wave, $V_{1,2}$ are the electron beam velocities, $a_{1,2}$ are the beam radii, and b is the beam tunnel radius, and ϵ are dielectric constants associated with each beam. This equation is derived and discussed in more detail in [1, 5]. Inserting a real frequency ω_r and solving this relationship for the imaginary part of the frequency ω_i yields the growth rate. It's notable that the theory neglects beam temperature/velocity spread, and builds in beam thickness via use of ϵ in an approximate way. Nevertheless, this expression for growth rate proved accurate for predicting simulated growth rates for thin beams and the velocity spreads examined here. A key point of the theory is that it does not predict when the growth will saturate and thus the maximum attainable efficiency.

3.3 Galaxy/Dakota Optimization of Theory to Produce Designs

This theory from Section 3.2 was used to aid in creating several of the amplifier designs we present. Some designs were generated via graphing the theory and visually selecting the curve that best matched goals and selecting the corresponding input parameters. For the designs using the optimization procedure, a program that calculated the theory was incorporated into the Galaxy [9] framework and the Dakota [10] nonlinear optimization package was applied to help select some of the beam parameters, similar to those in Table 2, that satisfied specific goals, such as maximizing the growth rate, subject to constraints, such as not having too much growth rate for frequencies that were not cut off in the waveguide. Central to optimization is characterizing how well the parameters suit your goals for the optimizing software. Dakota provides many nonlinear optimization algorithms.

In practice, this means designing a "cost function" which informs the optimization software, via a single number, how well the simulation performed. The optimization software then attempts to modify the input parameters to produce output that minimizes the cost function. Somewhat confusingly, we called our cost function $Merit$ and attempted to minimize that number. Equation (2) describes the procedure used to compute the cost function:

$$\begin{aligned} MeritGrowth &= -20 \times nineghzgrowth \\ MeritMaxGrowthFreq &= \begin{cases} 0, & maxgrowthfreq < 15GHz \\ \frac{(maxgrowthfreq - 15GHz)}{110MHz} & \text{otherwise} \end{cases} \\ Merit &= MeritGrowth + MeritMaxGrowthFreq \end{aligned} \tag{2}$$

In Equation (2), $nineghzgrowth$ is the growth rate computed at a real frequency of 9GHz, and $maxgrowthfreq$ is the real frequency at which the growth rate of the instability was computed to be a maximum. Here, the idea is to maximize the growth rate at 9GHz while enforcing a penalty for growth rates that peak above 15GHz. For the purposes of the optimization, the values input into the theory (namely some chosen subset of the beam parameters as in Table 2), were also constrained to make physical sense, in that we did not allow the beams to overlay each other or be too close to the wall. The 110MHz number in the denominator was an arbitrary choice that served to increase the penalty at

a particular rate above 15GHz. An example listing of a Python implementation that was used to guide the Galaxy/Dakota optimization is given in APPENDIX B.

4.0 RESULTS AND DISCUSSIONS

In this section we will show and discuss the results. We will identify where we have departed from the baseline parameters defined in Tables 1 and 2. Our work begins with (eventually mostly successful) attempts to reproduce the RTKA results from [1]. We had to make many assumptions, as described in Section 3.0, in our reproduction.

4.1 Reproduction of RTKA–the 3.375 GHz Design

The initial attempt at reproduction used the baseline parameters described in Tables 1 and 2. Also, we used a curved magnetic field dump and a perfectly matched layer (PML) to absorb any electromagnetic waves. Figure 4 shows the electron beams (in green) inserted on the left hand side. The red region on the right hand side is a PML, which functions to absorb any RF radiation that is generated. We also see that the annular beams begin changing direction to curve outward toward the wall at z=1.5m. This is necessary because PMLs do not gracefully absorb high current electron beams and will destabilize the simulation. The curvature was accomplished by introducing a magnetic field via a loop of current. At z=0.998m, the current was measured, Figure 5 was the result of this 2D simulation with no filtering of any kind. There is an extreme amount of noise present, and the magnitude of the current is seen to vary over a factor of 2, even though no RF signal was put in initially. On examination of the frequency characteristics of the noise, most of the noise signal was found to be above 15GHz, well beyond the frequencies expected to grow based on the theory. Instead the dominant causes of the noise were effects well-known to numerical modeling with PIC: particle shot noise, where noise simply due to finite number of particles is magnified by PIC particles each representing large numbers of electrons, and numerical Cerenkov radiation, where the numerical propagation speed of short wavelengths is nonphysically slow and thus such waves can interact nonphysically with the beam. To proceed with the design, we applied filtering techniques as described in Section 3.0.

Having successfully applied the numerical filtering and analysis techniques from Section 3.0, we were able to demonstrate a factor of 30 growth in $\tilde{I}$, which since power goes as the square of the current, implies a 900x growth in the RF power that could potentially be extracted from the beam. Figure 6 shows the maximum current modulation fraction when a small 3.375GHz signal was imposed at the input. This result is largely in agreement with the results reported in [1], though it is unclear if the referenced work used similar filtering methods to those used here, because the reference didn't include much discussion of the numerical techniques applied.

After successfully reproducing the 3.375GHz amplification results, we proceeded to work on more interesting X-band frequencies to see if the success could be repeated there.

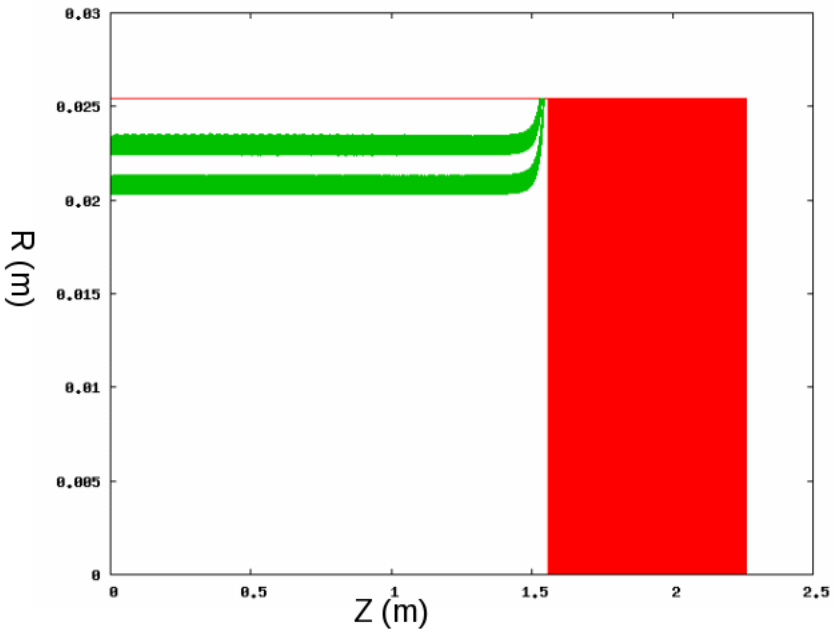

Figure 4: 3.375GHz Relativistic Two-stream Klystron Amplifier with Magnetic Field Dump

4.2 11.4GHz Design

The 11.4GHz design closely resembled [11], and differed largely in the beam and geometry parameters from the other two designs (3.375GHz and 9GHz). The base beam parameters are outlined in Table 2. However, shortly after beginning work on this design, the 11.4GHz design was abandoned, not because of lack of inherit merit that became clear at the time, but rather because 11.4GHz was less interesting from an application perspective than 9GHz. Nevertheless, we will present the 11.4GHz results that were obtained before our change in emphasis, results that have some merit. Figure 8 shows the theoretical growth rates as a function of frequency. Figure 9 shows the current modulation as a function of beam energies for an initial excitation amplitude of 0.005 on the high current beam. Appendix C, Section 7 has additional data on these designs.

4.3 9GHz Designs

Two attempts were made at a 9GHz design. Beam parameters, which differ from the baseline, are given in Table 3. Also, the designs discussed here used a 9.5mm beam tunnel radius, which implies a cutoff frequency of 12.1GHz for the TM_{01}mode, and used a beam tunnel length of 1.2m. The TM_{01}mode is considered the biggest risk for beam-wave interaction, as opposed to the transverse electric (TE) TE_{11}mode, which has a lower cutoff frequency but doesn't interact with the beam very strongly. The optimization procedures described in Section 3.3 were used to obtain the 9GHz theory curves shown in Figure 10. Also, for the 9GHz designs, the simulation was simplified by removing the magnetic beam

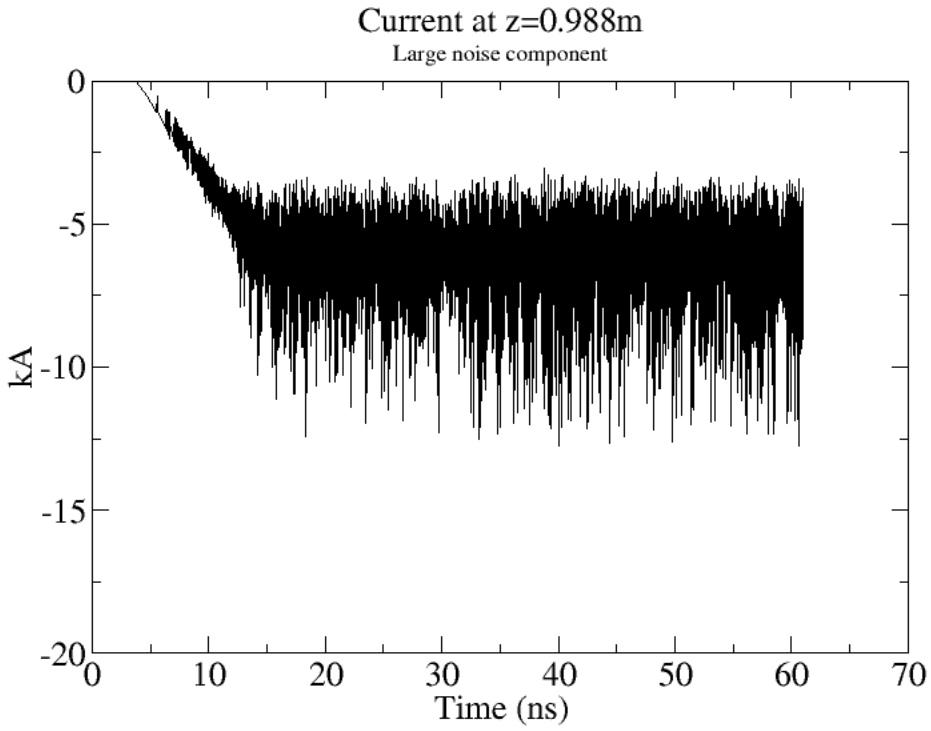

Figure 5: Current vs. Time for An Unfiltered 2D Simulation

dump and the perfectly matched layer on the right hand side. The reasoning was that the worst case for self-oscillation would be when there was no avenue for RF energy to escape the device, so replacement of the absorbing layer with a perfectly reflecting short was used to explore this extreme pessimistic case.

The first design attempted, #1, failed to deliver significant beam modulation in the length of the device. Elongation of the tube to increase amplification was possible, but not attempted because a longer device is less practical, so design #2 was attempted to increase the growth rate of the instability. The adjusted beam parameters allow for some growth above 12.1GHz, however, this was considered an acceptable trade given that 9GHz had failed to amplify in the previous design, and growth rates for the frequencies above cutoff are lower than ~.035, the growth rate for 9GHz in design #1.

Figure 11 shows a heat map of the maximum modulation fraction of the beam for the #2 9GHz design, where the maximum is the maximum fraction observed along the length of the device. Here, the beam tunnel was 1.2m long, and 9.5mm in radius. There was a 36dB gain in $\tilde{I}$, which delivers an $\tilde{I}$ magnitude that would theoretically allow 552MW assuming an optimistic 50% beam energy conversion efficiency. The low energy beam (Beam 1) had 83.4A of current, was 5mm in radius, 1mm thick, and had 168kV of beam energy after beam depression was calculated: the input beam energy is shown in the figure. The high energy beam had 3kA of current, 6.5mm in radius, 1mm thick, and had 368kV of beam energy after beam depression was calculated, again with input energies

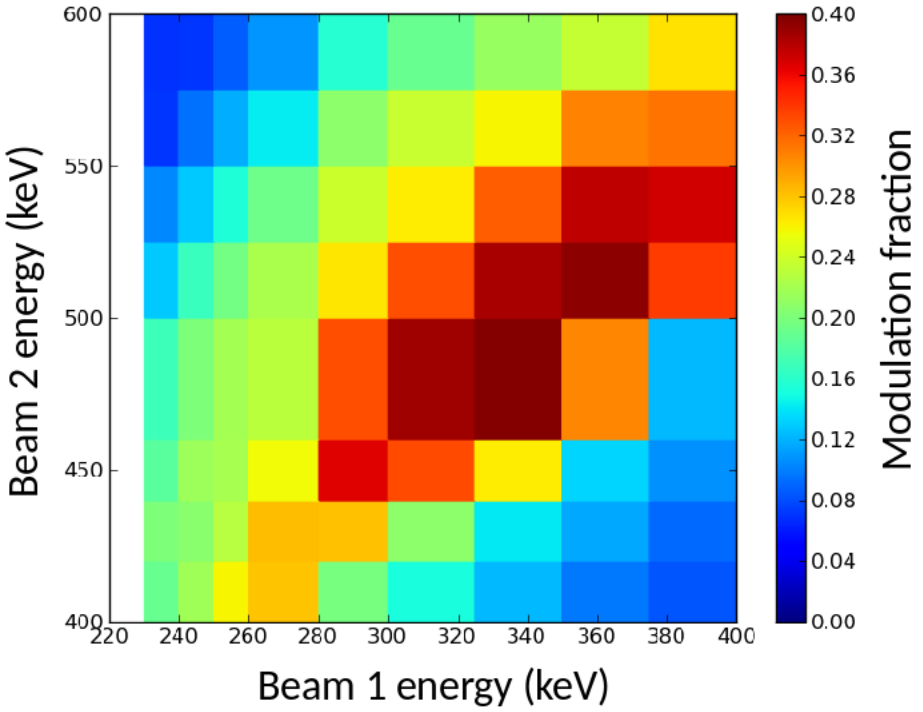

Figure 6: Maximum Current Modulation as a Function of Initial Beam Energies

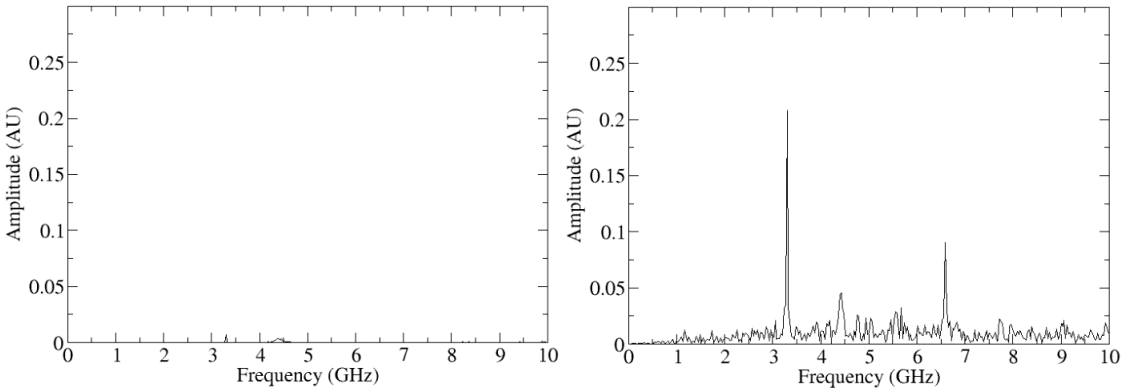

Figure 7: Fourier Transform of Current Modulation for z=5cm (Left) and z=1.5m (Right)

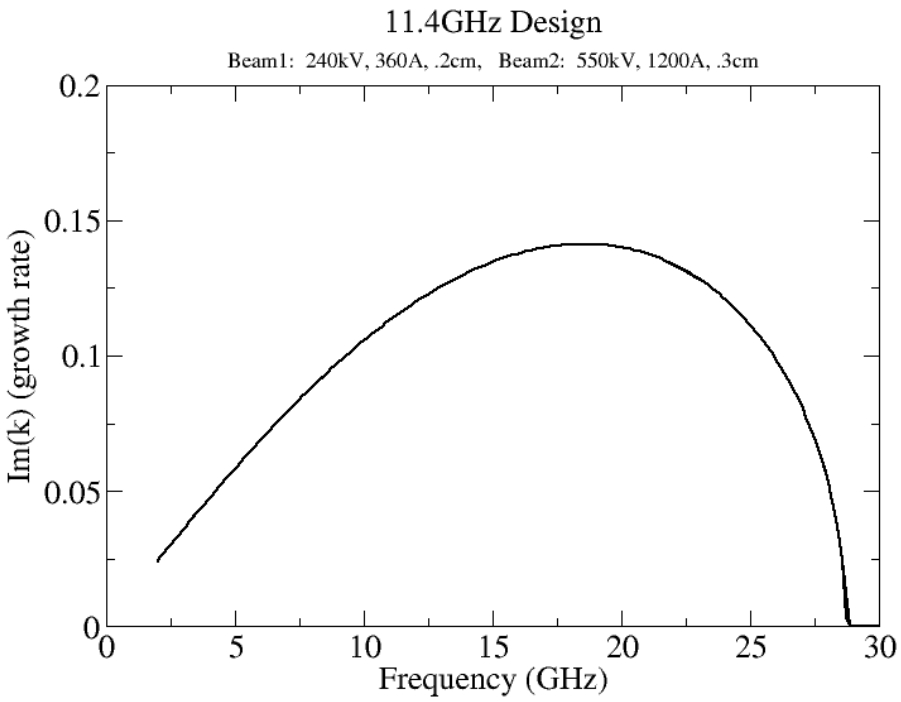

Figure 8: 11.4GHz Theory Curve

Table 3: 9GHz Electron Beam Parameters

Design	I_{bi}	V_{bi}	R_{bi}	t_{bi}	I_{bo}	V_{bo}	R_{bo}	t_{bo}
9GHz #1	50A	210kV	.227cm	1mm	3kA	450kV	.65cm	1mm
9GHz #2	83A	221kV	.513cm	1mm	3kA	450kV	.65cm	1mm

as shown in the figure. Theory curves for the two 9GHz designs are given in Figure 10: the discontinuities in the curves at around 1GHz are due to failure of the theory calculation to converge numerically and are not due to a physical effect: this part of the curve was ignored for the purposes of optimization and design. For additional results that are less relevant but which may also be useful, refer to APPENDIX C.

4.4 Electron Gun Design Attempts

Several types of electron gun designs were considered. A simple knife-edge “cookie cutter” beam emission design was eliminated for two reasons, first is that such designs typically have 8% beam energy spreads even at larger radii than are required here (which would worsen at lower radii), and that required emission current densities to emit a 3kA beam are far beyond the current state of the art.

Another candidate electron gun was a Friedman style gun [12]. This type of gun, shown in Figure 12, has the advantages of large cathode surface area and generates

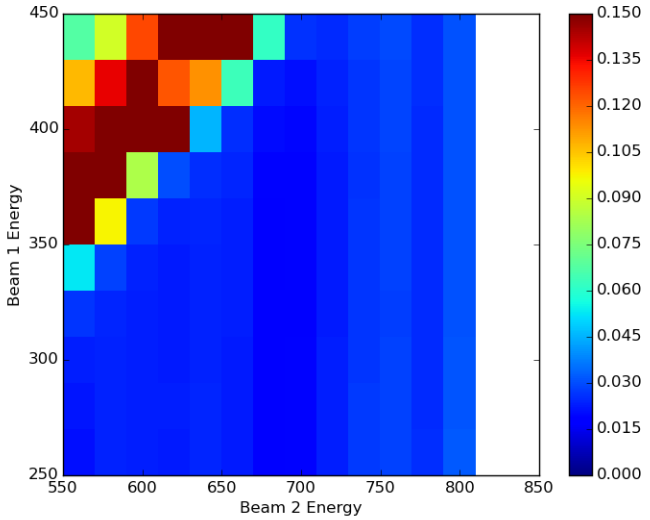

Figure 9: Maximum Current Modulation as a Function of Initial Beam Energies for 11.4GHz Design

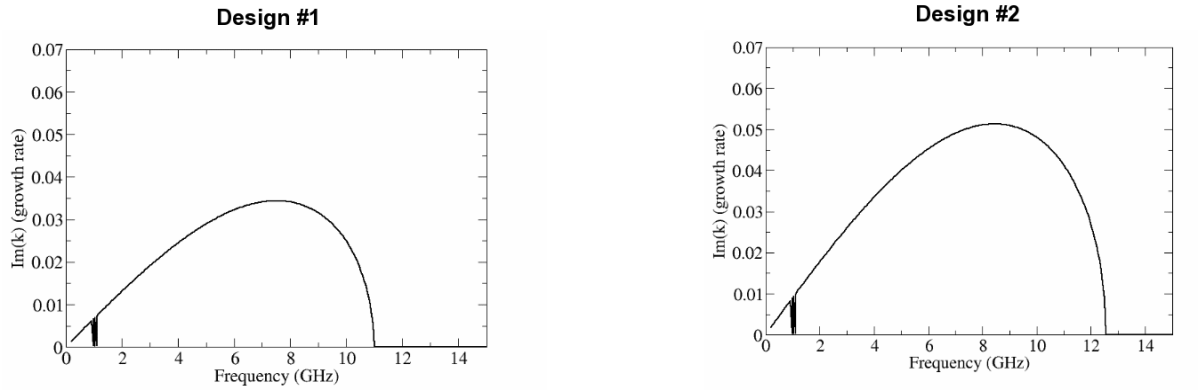

Figure 10: Theory Curves for 9GHz Designs

cold beams. Also, it requires a converging magnetic field, which will have the effect of diverting some beam energy into transverse rotational motion instead of the desired axial Z-directed motion. The more the beam is compressed, the more energy will end up in this rotational motion. For a gyrotron, this rotational motion is highly desired, but for our two-stream amplifiers, it is entirely unwanted and represents an energy sink. Another disadvantage of this type of gun is the annular thickness can be fairly large, it is difficult therefore to make a 1mm thick beam.

A third candidate is the Humphries electron gun [13], shown schematically in Figure 13. This gun features a cathode tip at a larger radius, which reduces the current density and thus produces a correspondingly colder beam. It also requires the beam to be compressed magnetically to maintain a reasonable current density on the cathode, again spinning up the beam and diverting energy into unwanted transverse rotational motion.

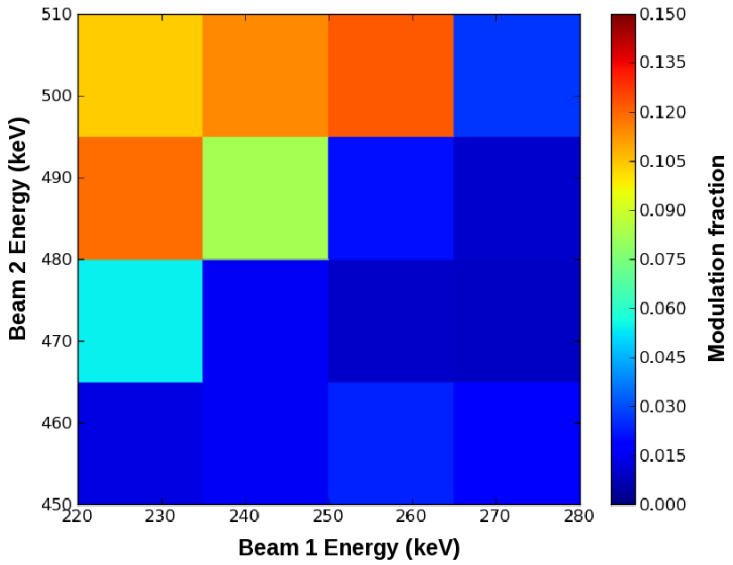

Figure 11: 9GHz Maximum Modulation Fraction as a Function of Initial Beam Energies

Also, this style of gun is difficult to make into a dual annular beam as is required for a two-stream amplifier.

To address the challenge of simultaneously producing both required beams, a hybrid design of a Friedman and Humphries type of gun was attempted, shown schematically in Figure 14. This gun used a Friedman style gun for lower current on the inner beam, a Humphries style gun for the outer beam, and attempted to minimize the convergence of the magnetic field. An inner conductor was also introduced to add more control over the electric fields at each of the guns. The procedure followed was to design the inner gun first.

The first attempt at the inner gun used a 5cm radius, and produced 1.7kA and had a launch voltage of 168kV. This is roughly a factor of 10x larger in radius than required, results are shown in Figure 15. Attempts at producing the requisite beam at the much smaller radius of 5mm proved challenging. To keep the current density at a level where plasma formation could be avoided the cathode surface area was kept to be nearly the same as the 50mm case. Results showed that even with this large surface area simulated current densities were still too high for a practical electron gun. However, this large cathode surface area caused dimensionality problems in the space required for the RTSA. As is shown in Figure 16, when a 5mm-radius electron beam gun was attempted the beam diverged, greatly exceeding the target annular radius of 1mm. The cathode size was not compatible with a 5mm beam radius. Several different magnetic field variations were used to compress the beam, but none were successful. The beam energy spread increased, and more energy went into unwanted transverse velocity components. The cathode surface area could have simply been scaled with the rest of the geometry, producing a similar beam as in Figure 15 at a 5mm radius. This electron gun would have worked in simula-

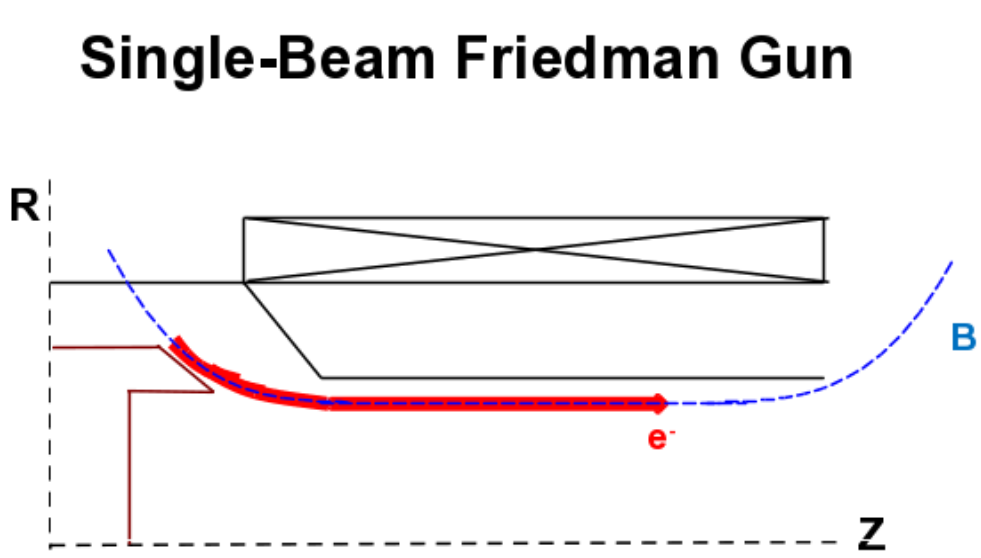

Figure 12: Friedman Type High Current Annular Electron Beam Gun

tion, but the current density required to produce such a beam from that size of a cathode would greatly exceed plasma formation limits, and would not function experimentally. To produce a beam of this intensity with this small a surface area, advanced electron-emiting materials are required.

The net result of the electron gun design effort was the elimination of all known candidate gun technologies as unable to meet the requirements.

4.5 Effect of Beam Energy Spread on Current Modulation

We were motivated to examine the effect of beam energy spread (beam temperature) on the performance of the relativistic two-stream amplifiers because previous non relativistic designs suffered efficiency loss [4] from the use of warm beams. While relativistic beams might be expected to suffer less from this difficulty, we found the effects of even very moderate beam energy spread to have strong impact, which has the net result of setting practical maximums on the allowable beam energy spreads to get reasonable performance.

Growth rate of the instability seems to be only moderately, if at all, impacted by the values of beam energy spread we tried. However, saturation (the peak current modulation fraction) seems to be strongly influenced. Figure 17 shows ICEPIC simulation of the current modulation fraction $|\tilde{I}|/I_{total}$as a function of distance down the beam tunnel from the beam launch for the #2 9GHz case from Section 4.3 with a .5% beam energy spread on the higher current beam. Here we see that the growth rate, at least initially, seems to follow theory for both cold and slightly warm beams. However, the slightly warm beam's modulation fraction saturates at a considerably lower peak value than the cold beam. Since extractable RF power is related to the square of the modulation fraction, ($P = I^2/Z$ where P is power, I is current and Z is a characteristic impedance) we would expect the

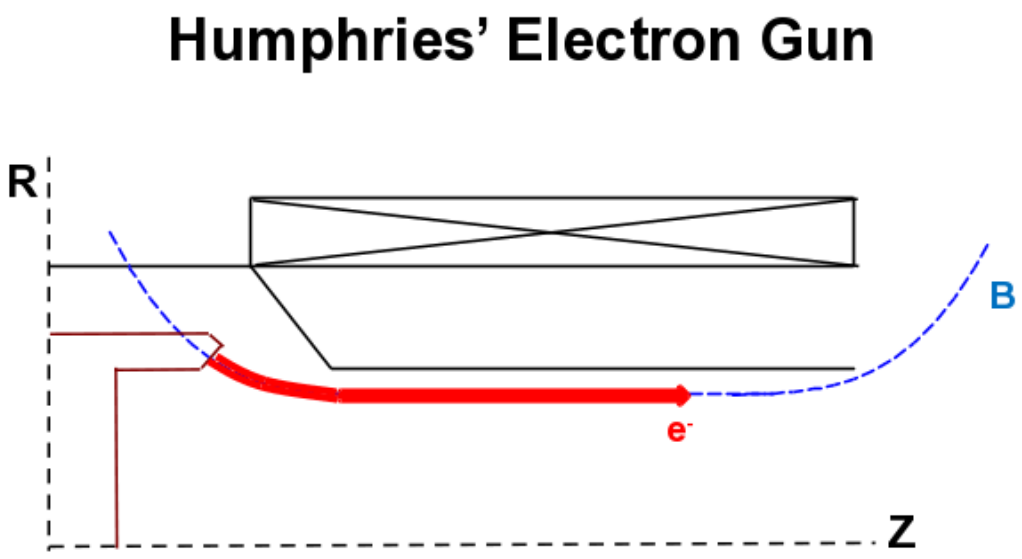

Figure 13: Humphries Type High Current Annular Electron Beam Gun

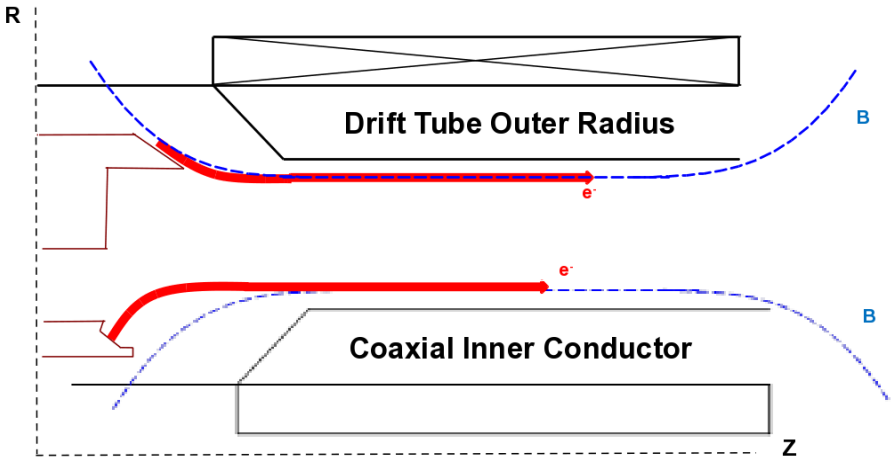

Figure 14: Hybrid Gun For Dual Annular Beam

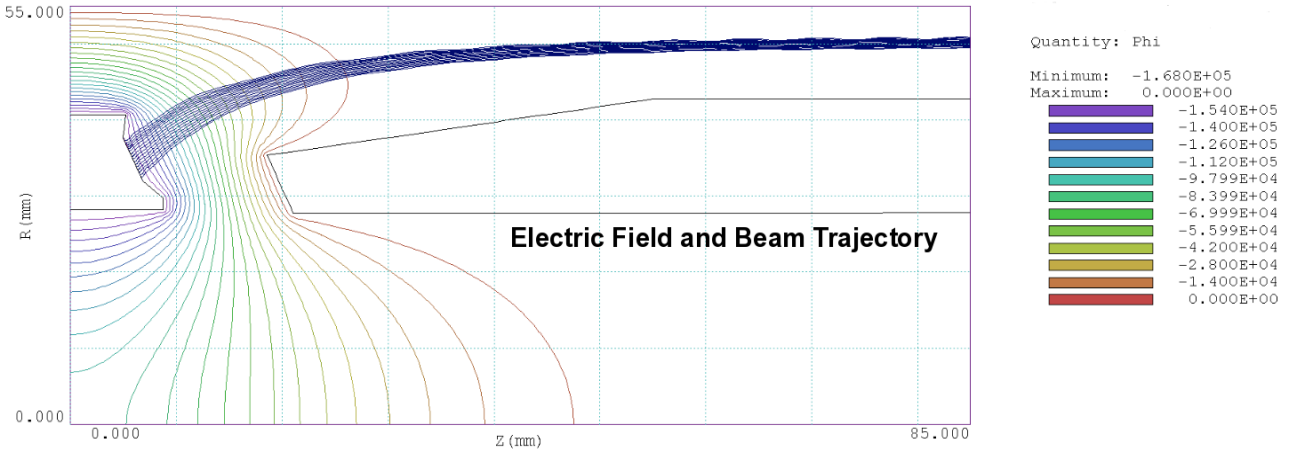

Figure 15: First Attempt At Inner Gun Design

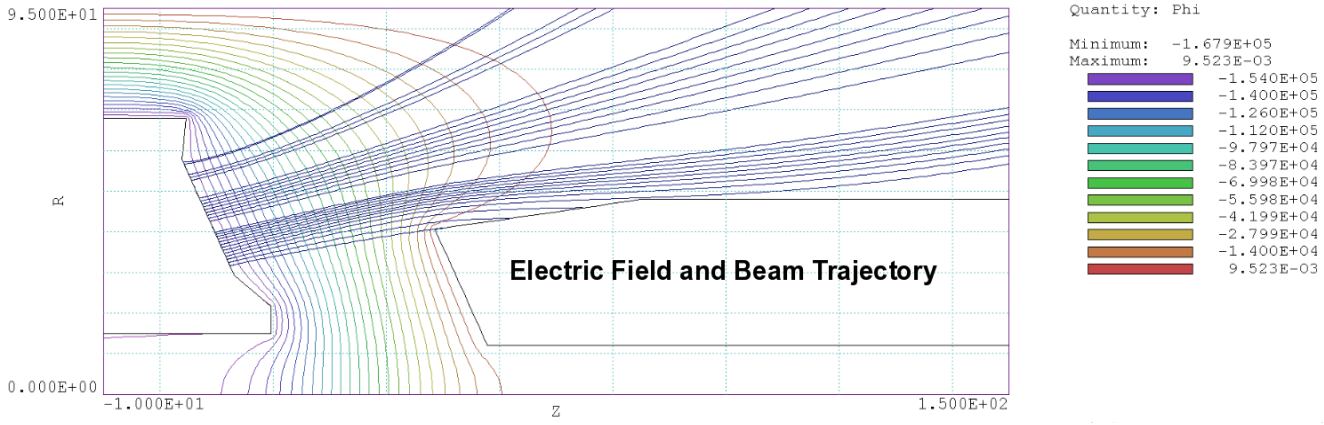

Figure 16: 5mm Radius Gun Produces Diverging Beam

warm beam to produce approximately $(.74/1.2)^2 = .38$, or less than 38% of the RF power of the cold beam. A reduced growth rate could be compensated for by lengthening the device, but the reduced maximum current modulation is not so readily remedied, and will result in reduced power output and reduced device efficiency.

Tables 4 and 5 show the impact of applying a beam temperature to the high current and low current beams respectively, holding the other beam cold (0% beam energy spread). Clearly, the energy spread of the higher current beam has the greater impact, but the effect of energy spread of the low current beam also has strong influence and cannot simply be ignored. Also, even a 1% beam energy spread severely reduces the maximum obtainable RF power. Furthermore, reducing the energy spread of the high current beam is considerably more difficult than reducing that of the low current beam.

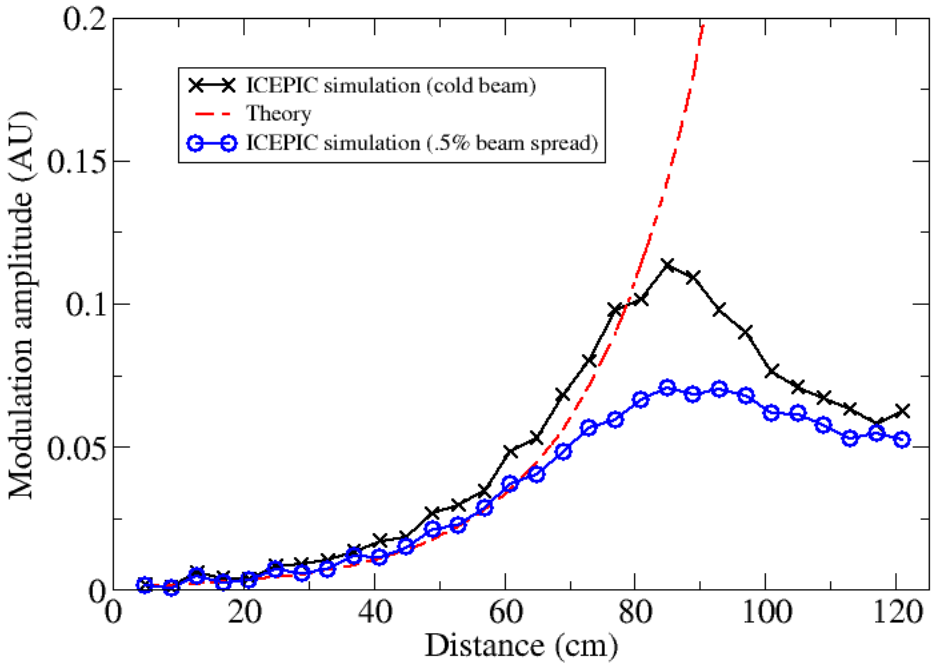

Figure 17: Modulation as a Function of Distance: Theory, Cold Beam, and 0.5% Beam Energy Spread

Table 4: Impact of High Current Beam Temperature on Current Modulation and Expected Power Performance

High current beam energy spread	$\|\tilde{I}\|/I_{total}$impact	Expected power impact
0.1%	-5%	-10%
0.25%	-11%	-21%
0.5%	-38%	-62%
1%	-60%	-84%

Table 5: Impact of Low Current Beam Temperature on Current Modulation and Expected Power Performance

Low current beam energy spread	$\|\tilde{I}\|/I_{total}$impact	Expected power impact
0.1%	-5%	-10%
0.25%	-10%	-19%
0.5%	-20%	-36%
1%	-43%	-68%

4.6 Effect of Increased Beam Thickness on Current Modulation

It is a considerable challenge to produce a kA-class annular beam that is only 1mm thick. Accordingly, we examined what performance impact it would have if the high current beam were expanded in annular thickness. We found that maintaining the beam's 1mm annular thickness was crucial for performance, as is shown in Table 6. Here, we see that if the beam is 2mm thick as opposed to 1mm thick, we cannot observe any modulation of the beam that is distinguishable from noise. While it may be possible to compensate for the increased beam thickness by adding more current, this again compounds the difficulty of producing the beam. Also, even a more moderate 50% beam thickness expansion reduced the expected maximum power output by 94%. The increases in beam thickness were chosen to have a practical impact on the difficulty of producing the required beams, but clearly the performance cost of relaxing the beam thickness requirements is very large, and would thus provide little relief to the difficulties of the electron gun designer.

Table 6: Impact of Beam Thickness on Current Modulation and Expected Power Performance

Beam annular thickness	$\lvert\tilde{I}\rvert/I_{total}$impact	Expected power impact
1mm	0%	0%
1.5mm	-75%	-94%
2mm	No modulation observed	No power expected
2.5mm	No modulation observed	No power expected

5.0 CONCLUSIONS

The essential concept, that of an amplifier using the two-stream instability to produce an amplifier, has been shown to work in simulation if high quality, low energy spread beams can be provided: in simulation, one simply specifies these. In reality, this is not at all straightforward.

Previous two-stream devices where plagued with low efficiency operation due to beam energy spreading, however, these studies didn't explore the regime of fairly highly relativistic beams (near 500KeV energy). The present study used simulations to discover just how much beam spreading is tolerable while preserving a reasonable amount of gain and efficiency. We found that a beam energy spread of even 1% had severe impact on both gain and efficiency, with 0.5% or less being actually desirable. Attempted beam gun designs to produce the requisite beams didn't come within an order of magnitude of current, and there are no obvious paths to improvement given available technology. Furthermore, the beam electrical requirements (energy spread, current, voltage) could not be met for these designs with any known electron gun design.

Additionally, the geometric constraints on the beams are very difficult to meet. If the two beams are not narrow enough in radius, the interaction weakens. If the two beams are not close enough radially, the interaction weakens. Producing very high current, for

example 3kA beams, that meet these constraints is challenging all by itself without the addition of beam energy spread requirements.

There are presently no known techniques for producing the requisite beams in the laboratory. A converging magnetic field will necessarily cause the beam's energy to divert partially, or even largely, into transverse velocity components, which cannot be exploited for energy conversion to RF via two-stream amplification, and thus represents a severe tax on overall efficiency. This compression process also tends to create longitudinal energy spread, which we have shown to be extremely deterimental. Contemporary cathode technology cannot provide the current density via immersing the cathodes in a uniform magnetic field. Furthermore, sharp edged cathodes have strong field nonuniformity at their edges, which causes a good deal of energy spread, 8% has been observed with this type of cathode at a lower current density.

Upcoming technologies, such as carbon nanotube cathodes, may provide such high current densities as to allow an immersed gun, or a gun with minimal converging magnetic compression, to meet the requirements. The two-stream broadband amplifier concept might be worth revisitation if the beams meet the requirements determined here.

Also unsolved, and unaddressed here in any way, is the issue of how to extract high power broadband RF efficiently from a bunched beam. For narrowband devices, this is a solved problem: resonant cavities (inherently somewhat narrowband) are excited by the bunched beam and the resulting RF power is extracted via waveguide. Low power broadband solutions exist: the helix is inherently broadband. However, the helix structure is also of little applicability for high power applications, for many reasons, the maximum power achieved with helix TWTs is 10 to 100kW. There are other broadband structures that the beam could interact with to convert its current modulation to RF energy, but these are not as compact as a resonant cavity, so there would be a lengthy amplification section followed by a lengthy conversion section. This is only a win if the conversion/extraction section plus the amplification section is smaller and more efficient than a traditional TWT, which tends to be more tolerant of beam energy spreading than is apparent with the two-stream concept.

At present, we recommend no further pursuit of a high power two-stream amplifier until the specific supporting technologies referred to above are developed: namely, techniques for producing very high current densities simultaneously with very precisely controlled beam energies and beam geometries, capable of producing multi-kA, ~500kV beams with radii less than 1cm and annular radial thickness of 1mm or less, and beam energy spreads of 0.5% or less.

6.0 REFERENCES

[1] C. Chen, P. Catravas, and G. Bekefi, "Growth and saturation of stimulated beam modulation in a two-stream relativistic klystron amplifier," *Applied physics letters*, vol. 62, no. 14, pp. 1579–1581, 1993.

[2] J. Pierce and W. Hebenstreit, "A new type of high-frequency amplifier," *Bell System Technical Journal*, vol. 28, no. 1, pp. 33–51, 1949.

[3] J. R. Pierce, "Double-stream amplifiers," *Proceedings of the IRE*, vol. 37, pp. 980–985, Sept 1949.

[4] P. M. Phillips, E. Zaidman, H. Freund, A. K. Ganguly, and N. R. Vanderplaats, "Review of two-stream amplifier performance," *IEEE Transactions on Electron Devices*, vol. 37, no. 3, pp. 870–877, 1990.

[5] C. Chen, "Efficiency scaling law for the two-stream amplifier," *Physics of Plasmas*, vol. 3, no. 8, pp. 3107–3110, 1996.

[6] R. E. Peterkin and J. W. Luginsland, "A virtual prototyping environment for directed-energy concepts," *Computing in Science & Engineering*, vol. 4, no. 2, pp. 42–49, 2002.

[7] J. P. Verboncoeur, A. B. Langdon, and N. Gladd, "An object-oriented electromagnetic pic code," *Computer Physics Communications*, vol. 87, no. 1-2, pp. 199–211, 1995.

[8] A. D. Greenwood, K. L. Cartwright, J. W. Luginsland, and E. A. Baca, "On the elimination of numerical cerenkov radiation in pic simulations," *Journal of Computational Physics*, vol. 201, no. 2, pp. 665–684, 2004.

[9] G. M. Stantchev, S. J. Cooke, J. J. Petillo, S. Ovtchinnikov, A. Burke, C. Kostas, D. Panagos, and T. M. Antonsen, "A high-performance distributed computing framework for parametric design optimization of rf devices," in *Plasma Science (ICOPS), 2016 IEEE International Conference on*, pp. 1–1, IEEE, 2016.

[10] S. Amini, B. Aminshahidy, and M. Afshar, "Simulation study of enhanced condensate recovery in a gas-condensate reservoir," *Iranian Journal of Chemical Engineering*, vol. 8, no. 1, pp. 3–14, 2011.

[11] V. M. C. Chen, "System for monitoring and analyzing manufacturing processes using statistical simulation with single step feedback," Feb. 17 1998. US Patent 5,719,796.

[12] M. Friedman and M. Ury, "Production and focusing of a high power relativistic annular electron beam," *Review of Scientific Instruments*, vol. 41, no. 9, pp. 1334–1335, 1970.

[13] S. Humphries and P. Ferguson, "Hollow-beam klystron design for the international linear collider," in *Pulsed Power Conference, 2007 16th IEEE International*, vol. 2, pp. 1368–1371, IEEE, 2007.

APPENDIX A EXAMPLE RTKA ICEPIC INPUT FILE

The ICEPIC input file shown below is representative of the ICEPIC input used to generate the data shown in this report. Values of variables and defaults were modified, and occasionally geometry was modified as well, as appropriate for the particular case.

```
; Parameters consistent with relativistic klystron amplifier

;RTKA reference,"Dispersioncharacteristicsofa Two-Stream Relativistic l;et.a
l.,Intense Microwave Pulses 1993
; RTSA reference, "Development of a highpower x-band relativistic two-stream

[Defaults]

BEAMTHICK = 0.001

DESIGN = 0    ; RTKA design
; DESIGN = 1   ; RTSA design
; Default beam parameters, appropriate for RTKA
      Beam1Energy = 220     ; kV
      Beam2Energy = 400     ; kV
      Beam1Current = 1000    ; Amp
      Beam2Current = 5000   ; Amp
      ;Beam1Rad = 0.0208      ; m  (beam radius)
      ;Beam2Rad = 0.0229      ; m  (beam radius)
      Beam1Rad = .021
      Beam2Rad = .023
      Beam1Thick = 0.001   ; m  (beam thickness)
      Beam2Thick = 0.001   ; m  (beam thickness)
      PulseLength = 10     ; ns
      BeamRiseTime = 25     ; ns
      Beam2ModFrac = 0.1    ; Initial beam2 modulation fraction

      B0z = .6              ; Guide field (T)

      Alpha = 0             ; Spin of beam (ratio of vperp to vparallel)

      INPUT_AMPLITUDE=200   ; arbitrary number for how big the input signal is.

      ; Drift tube
      InteractionLength=1.5 ; Interaction tube length (m)
      DriftTubeRadius = 0.0254 ; m
```

```
; Output Slow-Wave Structure
; For output, b(z) = b0 + b1*sin(2*PI*z/d)
Output_b0 = .035          ; m
Output_b1 = .007          ; m
Output_d  = 0.0092        ; m
OutputPeriods = 6       ; number of output periods

; Input characteristics  (coaxial)
InputFreq = 11.4          ; input frequency (GHz)
InputSize = .005          ; thickness, in radius, of input (m)
InputLength = .05         ; length of input segment (m)
InputAperture = .01       ; Size of input gap (m)

; Numerical parameters
LRes = 20           ; Cells per wavelength, along beam
TRes = 2            ; Cells per "BeamThickness"

INJECT=100

BEAM_RAMP=10e-9

BEAM_TEMPERATURE1 = 0    ;  temperature of beam, (fraction)
BEAM_TEMPERATURE2 = 0    ;  temperature of beam, (fraction)

RHS_PML=1    ; Right hand side PML

RippledWallOutput = 0    ;  Use a rippled wall output section

KlystronInput = 0     ;  use klystron-style input

; Resolution of output structure, in DXs:  how many DXs per segment
; This influences how many tapered cylinders are used to construct
; the rippled output section
OutputStructureResolution=1

; Simulation geometry
TWOD_RZ = 1

; Courant value
COURANT_VALUE=0.9

; Definitions for dumps
NUM_CURRENT_MODULATION_DUMPS = 30
```

```
;  Dump definitions

DUMP_PERIOD_PARTS = 5e-10

MAGNETIC_BEAM_DUMP = 1

WALL_CONDUCTIVITY=0    ; 0 actually means infinite, otherwise, MKS
WALL_EPSILON=10    ; 10 is approx. right for graphite

DIELECTRIC_BEAM_DUMP = 0


NEUTRAL_LAUNCH=0

USE_CONTROL_POINTS=0

XDMF_PART_DUMP=0

LHS_PML = 0

FILTERING = 1    ; 1 for friedman, 2 for godfrey
FILTERING_PARAM=0.2


[Variables]

;  Various designs

[IF] DESIGN==0
; Appropriate for RTKA
; Beam parameters
Beam1Energy = 220     ; kV
Beam2Energy = 400     ; kV
Beam1Current = 1000    ; Amp
Beam2Current = 5000   ; Amp
Beam1Rad = 0.0208      ; m  (beam radius)
Beam2Rad = 0.0229      ; m  (beam radius)
Beam1Thick = 0.001   ; m  (beam thickness)
Beam2Thick = 0.001   ; m  (beam thickness)

; Drift tube
InteractionLength=1.5 ; Interaction tube length (m)
DriftTubeRadius = 0.0254 ; m

InputFreq = 3.375         ; input frequency (GHz)
```

```
[ENDIF]

[IF] DESIGN==2
; Appropriate for RTKA
; Beam parameters
Beam1Energy = 220     ; kV
Beam2Energy = 400     ; kV
Beam1Current = 1000    ; Amp
Beam2Current = 5000   ; Amp
Beam1Rad = 0.0208      ; m  (beam radius)
Beam2Rad = 0.0225      ; m  (beam radius)
Beam1Thick = 0.001   ; m  (beam thickness)
Beam2Thick = 0.001   ; m  (beam thickness)

; Drift tube
InteractionLength=1.5 ; Interaction tube length (m)
DriftTubeRadius = 0.0254 ; m

InputFreq = 9.0         ; input frequency (GHz)

[ENDIF]

[IF] DESIGN==1

; Beam parameters
Beam1Energy = 240*1.58     ; kV
Beam2Energy = 550*1.29     ; kV
Beam1Current = 360    ; Amp
Beam2Current = 1200   ; Amp
Beam1Rad = 0.003      ; m  (beam radius)
Beam2Rad = 0.002      ; m  (beam radius)
Beam1Thick = 0.001   ; m  (beam thickness)
Beam2Thick = 0.001   ; m  (beam thickness)
PulseLength = 10     ; ns
BeamRiseTime = 25     ; ns

; Drift tube
InteractionLength=0.5 ; Interaction tube length (m)
DriftTubeRadius = 0.0095 ; m

InputFreq = 11.4         ; input frequency (GHz)

[ENDIF]
```

```
[IF] DESIGN==3

; Beam parameters
Beam1Energy = 240*1.58     ; kV
Beam2Energy = 550*1.29     ; kV
Beam1Current = 360    ; Amp
Beam2Current = 1200   ; Amp
Beam1Rad = 0.003      ; m  (beam radius)
Beam2Rad = 0.002      ; m  (beam radius)
Beam1Thick = 0.001   ; m  (beam thickness)
Beam2Thick = 0.001   ; m  (beam thickness)
PulseLength = 10     ; ns
BeamRiseTime = 25     ; ns

; Drift tube
InteractionLength=0.5 ; Interaction tube length (m)
DriftTubeRadius = 0.0095 ; m

InputFreq = 9         ; input frequency (GHz)

; Override some other defaults
DIELECTRIC_BEAM_DUMP=1
MAGNETIC_BEAM_DUMP=0

[ENDIF]

[IF] DESIGN==4

; Target beam energies
;
;Beam1Energy = 175     ; kV
;Beam2Energy = 450     ; kV
Beam1Current = 281    ; Amp
Beam2Current = 1000   ; Amp
Beam1Rad = 0.0015      ; m  (beam radius)
Beam2Rad = 0.0065      ; m  (beam radius)
Beam1Thick = 0.001   ; m  (beam thickness)
Beam2Thick = 0.001   ; m  (beam thickness)
PulseLength = 100     ; ns
BeamRiseTime = 25     ; ns

; Drift tube
InteractionLength=1.2 ; Interaction tube length (m)
DriftTubeRadius = 0.0095 ; m
```

```
InputFreq = 9          ; input frequency (GHz)

; Override some other defaults
DIELECTRIC_BEAM_DUMP=1
MAGNETIC_BEAM_DUMP=1
RHS_PML = 1


[ENDIF]


[IF] DESIGN==4

; Target beam energies
;
;Beam1Energy = 210      ; kV
;Beam2Energy = 450      ; kV
Beam1Current = 50     ; Amp
Beam2Current = 3000   ; Amp
Beam1Rad = 0.0025      ; m  (beam radius)
Beam2Rad = 0.0065      ; m  (beam radius)
Beam1Thick = 0.001   ; m  (beam thickness)
Beam2Thick = 0.001   ; m  (beam thickness)
PulseLength = 100     ; ns
BeamRiseTime = 25     ; ns

; Drift tube
InteractionLength=1.2 ; Interaction tube length (m)
DriftTubeRadius = 0.0095 ; m

InputFreq = 9          ; input frequency (GHz)

; Override some other defaults
DIELECTRIC_BEAM_DUMP=1
MAGNETIC_BEAM_DUMP=1
RHS_PML = 1


[ENDIF]


[IF] DESIGN==5

; Target beam energies
```

```
;
;Beam1Energy = 221     ; kV
;Beam2Energy = 450     ; kV
Beam1Current = 83.4    ; Amp
Beam2Current = 3000   ; Amp
Beam1Rad = 0.005       ; m  (beam radius)
Beam2Rad = 0.0065      ; m  (beam radius)
Beam1Thick = 0.001    ; m  (beam thickness)
Beam2Thick = 0.001    ; m  (beam thickness)
PulseLength = 100     ; ns
BeamRiseTime = 25     ; ns

; Drift tube
InteractionLength=1.2 ; Interaction tube length (m)
DriftTubeRadius = 0.0095 ; m

InputFreq = 9         ; input frequency (GHz)

; Override some other defaults
DIELECTRIC_BEAM_DUMP=1
MAGNETIC_BEAM_DUMP=1
RHS_PML = 1

[ENDIF]


[IF] DESIGN==6

; Target beam energies
;
;Beam1Energy = 221     ; kV
;Beam2Energy = 450     ; kV
Beam1Current = 83.4    ; Amp
Beam2Current = 3000   ; Amp
Beam1Rad = 0.005       ; m  (beam radius)
Beam2Rad = 0.0065      ; m  (beam radius)
Beam1Thick = 0.001    ; m  (beam thickness)
Beam2Thick = 0.001    ; m  (beam thickness)
PulseLength = 100     ; ns
BeamRiseTime = 25     ; ns

; Drift tube
InteractionLength=1.2 ; Interaction tube length (m)
DriftTubeRadius = 0.0095 ; m
```

```
InputFreq = 9          ; input frequency (GHz)

; Override some other defaults
DIELECTRIC_BEAM_DUMP=0
MAGNETIC_BEAM_DUMP=0
RHS_PML = 0

[ENDIF]

[IF] DESIGN==7
; Appropriate for RTKA
; Beam parameters
Beam1Energy = 220      ; kV
Beam2Energy = 400      ; kV
Beam1Current = 1000    ; Amp
Beam2Current = 5000    ; Amp
Beam1Rad = 0.0208      ; m  (beam radius)
Beam2Rad = 0.0225      ; m  (beam radius)
Beam1Thick = 0.001     ; m  (beam thickness)
Beam2Thick = 0.001     ; m  (beam thickness)

; Drift tube
InteractionLength=1.5 ; Interaction tube length (m)
DriftTubeRadius = 0.0254 ; m

InputFreq = 9.0          ; input frequency (GHz)
RHS_PML=0
MAGNETIC_BEAM_DUMP=0
DIELECTRIC_BEAM_DUMP=0

[ENDIF]



[IF] DESIGN==7
; Appropriate for RTKA
; Beam parameters
Beam1Energy = 220      ; kV
Beam2Energy = 400      ; kV
Beam1Current = 1000    ; Amp
Beam2Current = 5000    ; Amp
Beam1Rad = 0.0208      ; m  (beam radius)
Beam2Rad = 0.0225      ; m  (beam radius)
Beam1Thick = 0.001     ; m  (beam thickness)
```

```
Beam2Thick = 0.001   ; m  (beam thickness)

; Drift tube
InteractionLength=1.5 ; Interaction tube length (m)
DriftTubeRadius = 0.0254 ; m

InputFreq = 3.0         ; input frequency (GHz)
RHS_PML=0
MAGNETIC_BEAM_DUMP=0
DIELECTRIC_BEAM_DUMP=0

[ENDIF]



[IF] DESIGN==55

; Target beam energies
;
;Beam1Energy = 221     ; kV
;Beam2Energy = 450     ; kV
Beam1Current = 83.4    ; Amp
Beam2Current = 3000   ; Amp
Beam1Rad = 0.005       ; m  (beam radius)
Beam2Rad = 0.0065      ; m  (beam radius)
Beam1Thick = BEAMTHICK   ; m  (beam thickness)
Beam2Thick = BEAMTHICK   ; m  (beam thickness)
PulseLength = 100     ; ns
BeamRiseTime = 25     ; ns

; Drift tube
InteractionLength=1.2 ; Interaction tube length (m)
DriftTubeRadius = 0.0095 ; m

InputFreq = 9         ; input frequency (GHz)

; Override some other defaults
DIELECTRIC_BEAM_DUMP=1
MAGNETIC_BEAM_DUMP=1
RHS_PML = 1

[ENDIF]
```

```
; 3GHz design, RTKA-like
[IF] DESIGN==33
;Beam1Energy=220     ;kV
;Beam2Energy=450     ;kV
Beam1Current=500     ;A
Beam2Current=3000    ;A
Beam1Rad=0.013    ;m
Beam2Rad=0.016    ;m
Beam1Thick=BEAMTHICK  ;m
Beam2Thick=BEAMTHICK  ;m
PulseLength=100  ; ns
BeamRiseTime=25  ;ns
InteractionLength=1.5      ; m
DriftTubeRadius=.0254     ;
InputFreq = 3
RHS_PML=0
MAGNETIC_BEAM_DUMP=0
DIELECTRIC_BEAM_DUMP=0

[ENDIF]

PI=3.14152654
e=1.60219e-19
m=9.11e-31
e0 = 8.85e-12
c = 2.9979e8


; PML characteristics
PMLDepth = 8*2.99e8/InputFreq/1.0e9    ;  approximately 1/2 wavelength

OutputLength = OutputPeriods * Output_d

; Derived geometry parameters

; Input geometry parameters
InputInnerRadius = DriftTubeRadius + 0.002
InputOuterRadius = InputInnerRadius + InputSize

; total length
Ltotal = InteractionLength + OutputLength + PMLDepth

;  Maximum radius + a buffer
MaxRad = max(InputOuterRadius, Output_b0+Output_b1)
```

```
XMAX = MaxRad + .002
YMAX = XMAX
XMIN = 0
if TWOD_RZ==0: XMIN=-XMAX
YMIN = XMIN

;  Numerical parameters

; Mesh chosen to resolve wavelength
DZ = 2.99e8/InputFreq/1.0e9/LRes
Dtrans = min(Beam1Thick,Beam2Thick)/TRes
DZ = Dtrans
print "DZ=",DZ,"  Dtransverse=",Dtrans
Beam1Thick = max(Dtrans,Beam1Thick)
Beam2Thick = max(Dtrans,Beam2Thick)
SimulationTime = (PulseLength*1.1+BeamRiseTime*2)*1e-9

[IF] LHS_PML==0
ZMIN = 0
[ENDIF]
[IF] LHS_PML==1
ZMIN=-PMLDepth - 4*DZ
[ENDIF]
BEAMLAUNCHMIN = 0
ZMAX = Ltotal


; Output geometry parameters
OutputZStart = BEAMLAUNCHMIN + InteractionLength

; Control points

controlpoints=[Beam2Rad-Beam2Thick/2,Beam2Rad+Beam2Thick/2,Beam1Rad
               -Beam1Thick/2,Beam1Rad+Beam1Thick/2,DriftTubeRadius]
import string
controlpoints.sort()
;print controlpoints


; Definitions for dumps
Beam1Etot = Beam1Energy*e*1000 + m * c * c
Beam1Vel = c * sqrt(Beam1Etot**2 - (c**2*m)**2)/Beam1Etot
Beam2Etot = Beam2Energy*e*1000 + m*c*c
Beam2Vel = c * sqrt(Beam2Etot**2 - (c**2*m)**2)/Beam2Etot
```

```
;  Sanity checks
Beam1Density = Beam1Current / Beam1Vel / e /
              (pi * ((Beam1Rad+Beam1Thick/2.0)**2
              - (Beam1Rad-Beam1Thick/2.0)**2))
Beam1_Wp = sqrt(Beam1Density * e/e0*e/m)

Beam2Density = Beam2Current / Beam2Vel / e /
               (pi * ((Beam2Rad+Beam2Thick/2.0)**2
               - (Beam2Rad-Beam2Thick/2.0)**2))

Beam2_Wp = sqrt(Beam2Density * e/e0*e/m)


; Adjust the beam energy for alpha,
; so that we get the correct beam velocity in z based on the energy
[IF] Alpha != 0
print "Original beam energies:", Beam1Energy, Beam2Energy
gamm1new = 1.0 / sqrt(1. - ((1. + Alpha)*Beam1Vel/c)**2)
Beam1Energy = m * c * c / e *(gamm1new-1)/1000.0
gamm2new = 1.0 / sqrt(1. - ((1. + Alpha)*Beam2Vel/c)**2)
Beam2Energy = m * c * c / e *(gamm2new-1)/1000.0
print "Beam energies adjusted to keep
      Vparallel constant with given alpha:", Beam1Energy, Beam2Energy

[ENDIF]



print "n1 = ", Beam1Density, " n2 = ",Beam2Density
print "Wp1= ",Beam1_Wp,"  Wp2=",Beam2_Wp




; Calculate dT

[IF] TWOD_RZ==1
DT = 0.99*1./sqrt(1./(DZ*DZ)+1./(Dtrans*Dtrans))/3e8
[ENDIF]
[IF] TWOD_RZ==0
DT = 0.99*1./sqrt(1./(DZ*DZ)+2./(Dtrans*Dtrans))/3e8
[ENDIF]

print "DT = ", DT
```

```
;  Wp * dt check

print "Wp1*dt= ", Beam1_Wp*DT, "  Wp2*dt= ",Beam2_Wp*DT



[Time]
t_max = SimulationTime
;dt=DT
courant_value=COURANT_VALUE

[Partition]
axis=2
min_bal=100
max_bal=100000
bal_threshold=10

[Expert]
allow_protruding_shapes=1

[Cartesian]
in_units=mks
out_units=mks
; Some filtering of high frequencies.
[IF] FILTERING==1
theta=FILTERING_PARAM
[ENDIF]
[IF] FILTERING==2
alpha=0.125
max_count=2
[ENDIF]
default_b = (0,0,B0z)
[IF] TWOD_RZ==1
coord_system=1
ig_dir=(0,1,0)
[ENDIF]

[XGrid1]
range=Uniform(XMIN,XMAX+Dtrans, int((XMAX-XMIN)/Dtrans)+1)
[IF] USE_CONTROL_POINTS==1
control_points = '('+repr(len(controlpoints))+
                 ","+string.join(map(repr,controlpoints),",")+')'
[ENDIF]

[IF] TWOD_RZ==0
```

```
[YGrid1]
range=Uniform(YMIN, YMAX, int((YMAX-YMIN)/Dtrans))
[ENDIF]

[IF] TWOD_RZ==1
[YGrid1]
range=Uniform(0,1.0,1)
[ENDIF]

[ZGrid1]
range=Uniform(ZMIN-DZ, ZMAX+DZ, int((ZMAX-BEAMLAUNCHMIN)/DZ )+2)

[Variables]
print "Freq. res of mesh:", 3e8/DZ/1e9/2.0



; Geometry definition

; Basic drift tube
[ShapeN]
label1=DriftTube
shape=Cylinder(0,0,BEAMLAUNCHMIN,0,0,ZMAX,DriftTubeRadius)
material=0


[IF] KlystronInput==1
; Input section, coaxial part
[ShapeN]
label1=InputSection
shape=Cylinder(0,0,BEAMLAUNCHMIN,0,0,BEAMLAUNCHMIN+InputLength,
        InputOuterRadius,InputInnerRadius)
material=0

; Input section, coupling aperture
[ShapeN]
label1=InputSection
shape=Cylinder(0,0,BEAMLAUNCHMIN+InputLength-InputAperture,
            0,0,BEAMLAUNCHMIN+InputLength,InputOuterRadius)
material=0

[ENDIF]

[IF] MAGNETIC_BEAM_DUMP==1
EVAL print "Turning on magnetic field dump."
```

```
[LoopN]
axis=(0,0,1)
btarget = -B0z/2
bcomp=2
refpoint = (0,0,ZMAX-DZ-PMLDepth)
bapp_mode=0
nsegs=64
radius = DriftTubeRadius+10*DZ
center=(0,0,ZMAX-DZ-PMLDepth)

[ENDIF]



; Input signal launch



[IF] KlystronInput==1

[BoundN]
method=TE_MODE
shape=Cylinder(0,0,BEAMLAUNCHMIN+PMLDepth-0.5*DZ,0,0,
        BEAMLAUNCHMIN+PMLDepth+0.5*DZ,InputOuterRadius,InputInnerRadius)
modes=0,0,0,0
frequency = InputFreq * 1e9
mode_coeff=INPUT_AMPLITUDE
trans_dir=1
dir=2
amp0 = 0
amp1 = 1
amp2 = 0
flattop = (PulseLength-100)*1e-9
ramp = 1e-8
rampdown = 1e-8
;tstart=1e-8
tstart=0
tstop = (PulseLength-100)*1e-9 + 1e-8
sweep=1e9

; Input PML
; PML
[BoundN]
method=PML
dir=2
```

```
mode=WR-90
shape=Cylinder(0,0,BEAMLAUNCHMIN-DZ/2,0,0,BEAMLAUNCHMIN+DZ/2,
        InputOuterRadius,InputInnerRadius)
rdepth=PMLDepth-4*DZ



; Input power measurement
[DumpN]
dump_format=POWER
dump_name=PWR_IN
dump_plane=2
dump_value=BEAMLAUNCHMIN+4*DZ+PMLDepth
shape=Cylinder(0,0,BEAMLAUNCHMIN+PMLDepth+2*DZ,0,0,
        BEAMLAUNCHMIN+6*DZ+PMLDepth,InputOuterRadius,InputInnerRadius)


[ENDIF]


[IF] WALL_CONDUCTIVITY != 0
;Create a dielectric to launch from
;[MaterialN]
;sigma=WALL_CONDUCTIVITY
;name=wall_material
;epsilon=WALL_EPSILON

[BoundN]
method=RESISTIVE
conductivity=WALL_CONDUCTIVITY
shape = Cylinder(0,0,ZMIN,0,0,InteractionLength,DriftTubeRadius+2*DZ)



[IF] LHS_PML==1
; Set up for launching after a left hand side PML

; Set up a volume for a PML on the LHS
[ShapeN]
material=0
shape=Cylinder(0,0,ZMIN,0,0,BEAMLAUNCHMIN,DriftTubeRadius)

; Create the PML
[BoundN]
```

```
method=PML
dir=2
mode=WR-90
shape=Cylinder(0,0,ZMIN-DZ/2,0,0,ZMIN+DZ/2,DriftTubeRadius)
rdepth=PMLDepth-4*DZ

;Create a dielectric to launch from
[MaterialN]
sigma=0
mu=1
epsilon=1.000001
name=TenuousDielectric_Input




[ShapeN]
shape=Cylinder(0,0,BEAMLAUNCHMIN-2*DZ,0,0,BEAMLAUNCHMIN,DriftTubeRadius)
material=TenuousDielectric_Input

; Power dump on LHS

[DumpN]
dump_format=POWER
dump_name=PWR_LEFT
dump_plane=2
dump_value=BEAMLAUNCHMIN-3*DZ

[ENDIF]


[IF] RippledWallOutput==1
;  Output section, rippled wall

[Repeat]
Rtype = "Shape"
Rindex = 0
Rmaxindex = OutputLength
Rstep = OutputStructureResolution*DZ
[BeginRepeating]
EVAL rsz = 2*3.141592654*Rindex/Output_d
EVAL rl = Output_b0 + Output_b1 * sin(rsz)
EVAL rsz2 = 2*3.141592654*(Rindex+Rstep)/Output_d
EVAL rr = Output_b0 + Output_b1 * sin(rsz2)
```

```
EVAL zl = OutputZStart+Rindex
EVAL zr = zl + Rstep
material=0
label1=OutputSection
shape=Tap_Cylinder(0,0,zl,0,0,zr,rl,rr)

[EndRepeat]

[ENDIF]

[IF] RippledWallOutput==0
;  Continuation of drift tube to output
[ShapeN]
shape=Cylinder(0,0,OutputZStart,0,0,OutputZStart+OutputLength,
                DriftTubeRadius)
material=0

[Variables]
rr = DriftTubeRadius
zr = OutputZStart+OutputLength

[ENDIF]




;  PML shape

[ShapeN]
material=0
shape=Cylinder(0,0,zr,0,0,ZMAX,rr)
[IF] RHS_PML==1
; PML
[BoundN]
method=PML
dir=2
mode=WR-90
shape=Cylinder(0,0,ZMAX-DZ/2,0,0,ZMAX+DZ/2,rr)
rdepth=PMLDepth-4*DZ
[ENDIF]

; Output power diagnostic, right before PML
[DumpN]
dump_format=POWER
dump_plane=2
```

```
dump_value=ZMAX-PMLDepth-DZ
dump_name=PWR_OUT

[IF] DIELECTRIC_BEAM_DUMP==1

[MaterialN]
sigma=0
epsilon=1.00001
name=beam_stop_dielectric

; Beam stopper dielectric
[ShapeN]
shape=Cylinder(0,0,ZMAX-PMLDepth-3*DZ,0,0,ZMAX-PMLDepth-2*DZ,rr)
material=beam_stop_dielectric

[ENDIF]

; Particles, and beam stopper secondary emission

[ParticlesN]
method=SPECIES
species_name=BEAM_ELECTRONS
shape=Cylinder(0,0,BEAMLAUNCHMIN,0,0,ZMAX,XMAX)

[ParticlesN]
method=SPECIES
species_name=MASSIVE_ELECTRONS
shape=Cylinder(0,0,BEAMLAUNCHMIN,0,0,ZMAX,XMAX)
q=-e
qtom=-e

[IF] DIELECTRIC_BEAM_DUMP==1
; Secondary particle tosser-outer
; Hugely massive (so unmagnetized) particle with charge of electron
[ParticlesN]
method=SECONDARY
shape=Cylinder(0,0,ZMAX-PMLDepth-4.5*DZ,0,0,ZMAX-PMLDepth-DZ,rr)
sec_threshold=0
sec_coefficient=1
sec_refl=-1
species_name=BEAM_ELECTRONS
second_species_name=MASSIVE_ELECTRONS

[ENDIF]
```

```
;   Beams

; We are implementing a neutral launch

[ParticlesN]
method=SPECIES
species_name=MASSIVE_POSITRONS
shape=Cylinder(0,0,BEAMLAUNCHMIN,0,0,BEAMLAUNCHMIN+DZ,Beam1Rad)
q=e
qtom=e


[IF] Beam1Current > 0
[ParticlesN]
method=BEAM
random=1
shape=Cylinder(0,0,BEAMLAUNCHMIN-1.1*DZ,0,0,BEAMLAUNCHMIN+1.1*DZ,
        Beam1Rad+Beam1Thick/2.0,Beam1Rad-Beam1Thick/2.0)
energy = Beam1Energy*1000
dir=2
alpha = Alpha
axis1 = (0, 0, 0)
axis2 = (0, 0, 1)
current = Beam1Current
temp = Beam1Energy * 1000 * BEAM_TEMPERATURE1
species_name=BEAM_ELECTRONS
ramp=BEAM_RAMP
inject=INJECT
[ENDIF]

[IF] Beam2Current > 0

[ParticlesN]
method=BEAM
random=1
shape=Cylinder(0,0,BEAMLAUNCHMIN-1.1*DZ,0,0,BEAMLAUNCHMIN+1.1*DZ,
        Beam2Rad+Beam2Thick/2.0,Beam2Rad-Beam2Thick/2.0)
energy = Beam2Energy*1000
dir=2
alpha = Alpha
axis1 = (0, 0, 0)
axis2 = (0, 0, 1)
current=Beam2Current
species_name=BEAM_ELECTRONS
ramp=BEAM_RAMP
```

```
inject=INJECT
temp = Beam2Energy * 1000 * BEAM_TEMPERATURE2
ncoeff=2
c0 = 1
c1 = Beam2ModFrac
frequency=InputFreq * 1e9

[ENDIF]

[IF] NEUTRAL_LAUNCH==1
; Arrange for a neutral-ish launch of these beams
[ParticlesN]
method=BEAM
shape=Cylinder(0,0,BEAMLAUNCHMIN-1.1*DZ,0,0,BEAMLAUNCHMIN+1.1*DZ,
               Beam2Rad+Beam2Thick/2.0,Beam2Rad-Beam2Thick/2.0)
energy = 6.03e35
vector = (1,0,15)
ramp=BEAM_RAMP
current=Beam2Current
species_name=MASSIVE_POSITRONS

; Arrange for a neutral-ish launch of these beams
[ParticlesN]
method=BEAM
shape=Cylinder(0,0,BEAMLAUNCHMIN-1.1*DZ,0,0,BEAMLAUNCHMIN+1.1*DZ,
               Beam1Rad+Beam1Thick/2.0,Beam1Rad-Beam1Thick/2.0)
energy = 6.03e35
vector = (1,0,15)
ramp=BEAM_RAMP
current=Beam1Current
species_name=MASSIVE_POSITRONS

[ENDIF]

[DumpN]
dump_format=GRID
dump_plane=1
dump_value=0
dump_name=grid_rz

[DumpN]
dump_format=PARTB
dump_period=DUMP_PERIOD_PARTS
dump_interval=5000
num_sample=10
```

```
species_dump=1
species_name=BEAM_ELECTRONS
dump_name=part_beam
[IF] TWOD_RZ==0
num_sample = 100
[ENDIF]


[IF] XDMF_PART_DUMP==1
[DumpN]
dump_format=XDMF_PARTICLES
dump_period=DUMP_PERIOD_PARTS
dump_interval=100000
num_sample=100
species_dump=1
species_name=BEAM_ELECTRONS
dump_name=part_beam_xdmf
[ENDIF]


[IF] DIELECTRIC_BEAM_DUMP==1
[DumpN]
dump_format=PART
dump_period=DUMP_PERIOD_PARTS
;dump_interval=1
num_sample=0
species_dump=1
species_name=MASSIVE_ELECTRONS
dump_name=part_dump

[ENDIF]

[IF] NEUTRAL_LAUNCH==1

[DumpN]
dump_format=PART
dump_period=DUMP_PERIOD_PARTS
;dump_interval=1
num_sample=0
species_dump=1
species_name=MASSIVE_POSITRONS
dump_name=part_launch

[ENDIF]
```

```
[DumpN]
dump_format=XDMF_FIELDS
dump_interval=10000
dump_name=all_fields
fieldflags=2-2-2-0-0-0
nstart=0

[DumpN]
dump_format=MESH
num_sample=1

; Monitor current modulation in the beam tunnel
;[Repeat]
;Rtype = "Dump"
;Rindex = BEAMLAUNCHMIN+InputLength
;Rmaxindex = BEAMLAUNCHMIN+InputLength+InteractionLength
;Rstart = 0
;Rstep = InteractionLength/NUM_CURRENT_MODULATION_DUMPS
;[BeginRepeating]
;dump_name = "CurrentModInBeamTunnel_Z=" + repr(Rindex)
;dump_format = CUR_J
;dump_plane=2
;dump_value=Rindex
;[EndRepeat]

; Monitor current modulation in the beam tunnel
[Repeat]
Rtype = "Dump"
Rindex = BEAMLAUNCHMIN+InputLength
Rmaxindex = BEAMLAUNCHMIN+InputLength+InteractionLength
Rstart = 0
Rstep = InteractionLength/NUM_CURRENT_MODULATION_DUMPS
[BeginRepeating]
dump_name = "Current2ModInBeamTunnel_Z=" + repr(Rindex)
flush=25000
dump_format = CUR_CIR
dump_plane=2
p = (0,0,Rindex)
rad = DriftTubeRadius-2.5*Dtrans
num_sample=128
[EndRepeat]
```

APPENDIX B PYTHON PROGRAM FOR GALAXY OPTIMIZATION

The Python program below was used to compute the 'cost function' or 'merit value' for how well a theory curve met design objectives. These results were fed into Galaxy/DAKOTA optimization to select parameters for simulation.

```
#!/usr/bin/env python

import os
import sys
import string
from math import *

def MeritCurve(nineghzgrowth, maxgrowthfreq):
      MeritGrowth = -20.0 * nineghzgrowth
      if maxgrowthfreq < 1.5e10:
            MeritMaxGrowthFreq = 0
      else:
            MeritMaxGrowthFreq = (maxgrowthfreq - 1.5e10)/1.1e8
      # stiffened this
      Merit = MeritGrowth+MeritMaxGrowthFreq
      return (Merit, MeritGrowth, MeritMaxGrowthFreq)

# program reads in output from Jack Watrous's
# theory program and extracts some
# information about the Im(K) curve:
#  1)  Maximum growth rate
#  2)  9GHz growth rate
#  3)  maximum frequency with non-zero growth rate

def read_data(fh):
      line = fh.readline()

      maxgrowthrate = -1.0
      maxgrowthratefrequency = -1.0
      nineghzgrowth = -1.0
      maxgrowthfreq = -1.0
      while line != "":
            try:
                  fields = map(float,string.split(line))
                  imk = fields[1]
                  frequency = fields[0]
            except Exception:
                  line = fh.readline()
                  continue
```

```
            maxgrowthrate = max(maxgrowthrate, imk)
            if maxgrowthrate == imk:  maxgrowthratefrequency = frequency
            if frequency > 9.0e9 and nineghzgrowth==-1.0:
                  nineghzgrowth = imk
            if imk > 1.0e-6:
                   maxgrowthfreq = frequency
            line = fh.readline()
      return (maxgrowthrate, maxgrowthratefrequency,
              nineghzgrowth, maxgrowthfreq)

def main():
      try:
            f = open(sys.argv(1),"r")
      except Exception:
            f = sys.stdin

      (maxgrowthrate, maxgrowthratefrequency, ninghzgrowth,
       maxgrowthfreq) = read_data(f)
      print "Max growth rate: ", maxgrowthrate,
      " at frequency (GHz):  ", maxgrowthratefrequency/1.0e9
      print "9GHz growth rate: ", nineghzgrowth
      print "Maximum frequency with nonzero growth: (GHz)",
      maxgrowthfreq/1.0e9
      print nineghzgrowth, maxgrowthfreq/1.0e9, maxgrowthrate,
      maxgrowthratefrequency/1.0e9
      print MeritCurve(nineghzgrowth, maxgrowthfreq)


if __name__ == '__main__':
      main()
```

APPENDIX C RESULTS NOT PRESENTED IN THE MAIN BODY

This Appendix contains results that were not reported in the body of this report, but that may nevertheless be of use.

1.0 Theory Curve for 1kA, 9GHz Design

Figure C-1 shows the results of a theory calculation for a 9GHz design which used a 1kA main beam instead of a 3kA beam. Parameters are listed in Table C-1. Pursuit of this design was attempted to relax the requirements on the gun design from 3kA to 1kA, however, the achieved growth rate was too low to be interesting for a device of a practical length. The wall radius was 9.5mm.

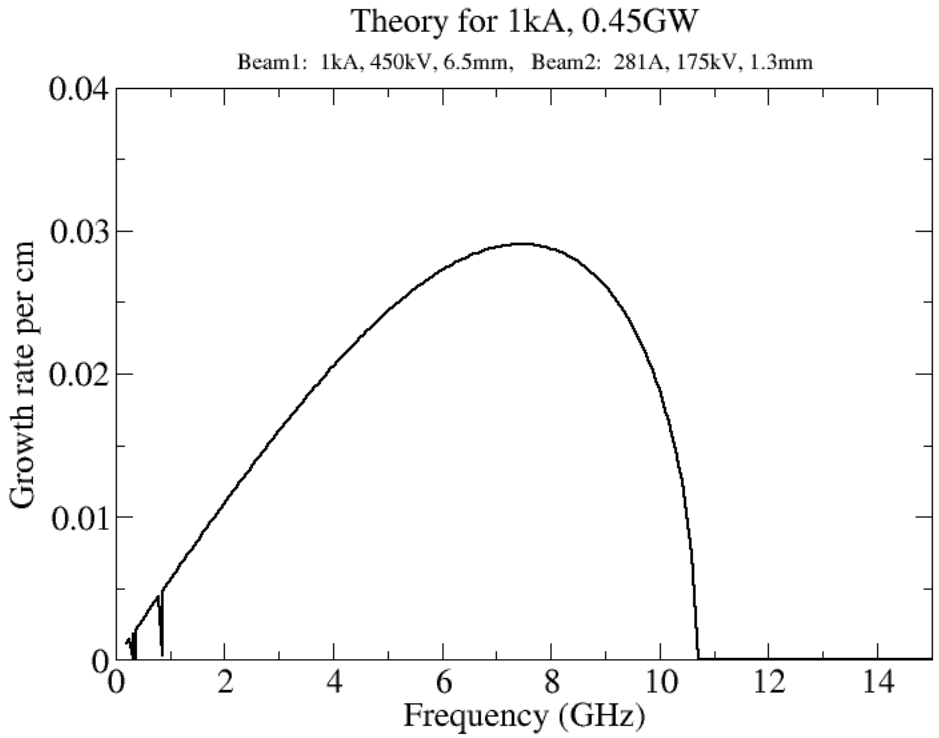

Figure C-1: Theory Curve For 1kA Design

Table C-1: 9GHz, 1kA Electron Beam Parameters

Design	I_{bi}	V_{bi}	R_{bi}	t_{bi}	I_{bo}	V_{bo}	R_{bo}	t_{bo}
9GHz, 1kA	281A	175kV	.13cm	1mm	1kA	450kV	.65cm	1mm

2.0 Theory Curve Family for Varying Values of Current on Beam 2

The theory curves in Figure C-2 illustrate the effect on the growth rate curves of varying the current of the high current beam. The values B2C are beam currents in kA, other parameters of the beam are shown in Table C-2, and the tube radius was 0.95cm. These designs were not tested via PIC simulation, peak growth frequencies above the general region of 9GHz weren't the target of design.

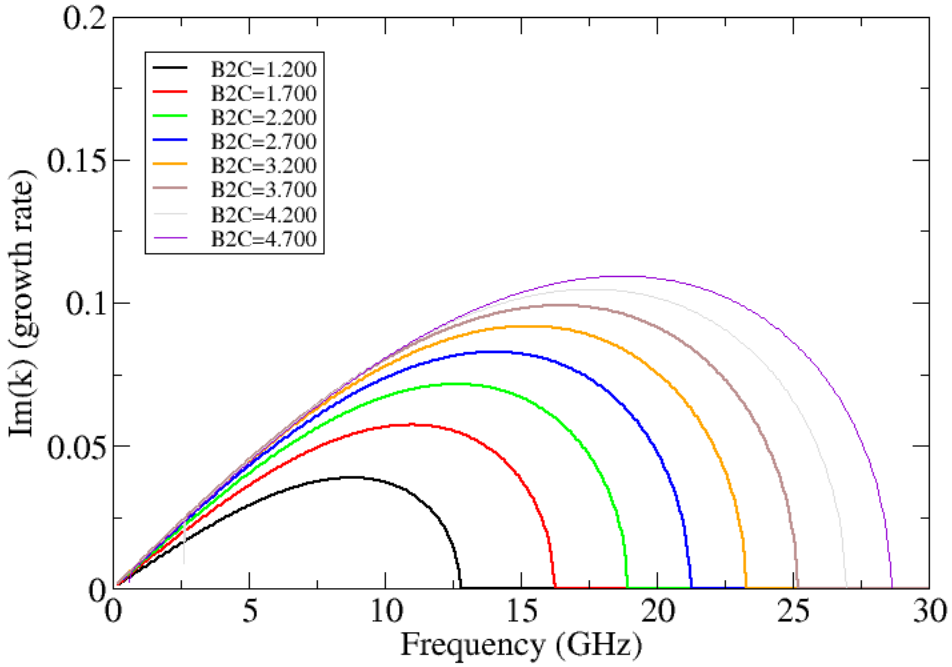

Figure C-2: Family Of Curves For Varying Beam Currents

Table C-2: Electron Beam Parameters For Beam 2 Current Scan

Design	I_{bi}	V_{bi}	R_{bi}	t_{bi}	I_{bo}	V_{bo}	R_{bo}	t_{bo}
Various beam 2 currents	360A	240kV	.45cm	1mm	see plot	500kV	.65cm	1mm

3.0 Effect of Varying Beam Radius

The theory curves in Figure C-3 illustrate the effect of varying the radii of the low current, inner beam. The values B1R are in cm, other beam parameters are listed in Table C-3, and the beam tunnel was 0.95cm in radius. These designs were not tested via PIC simulation.

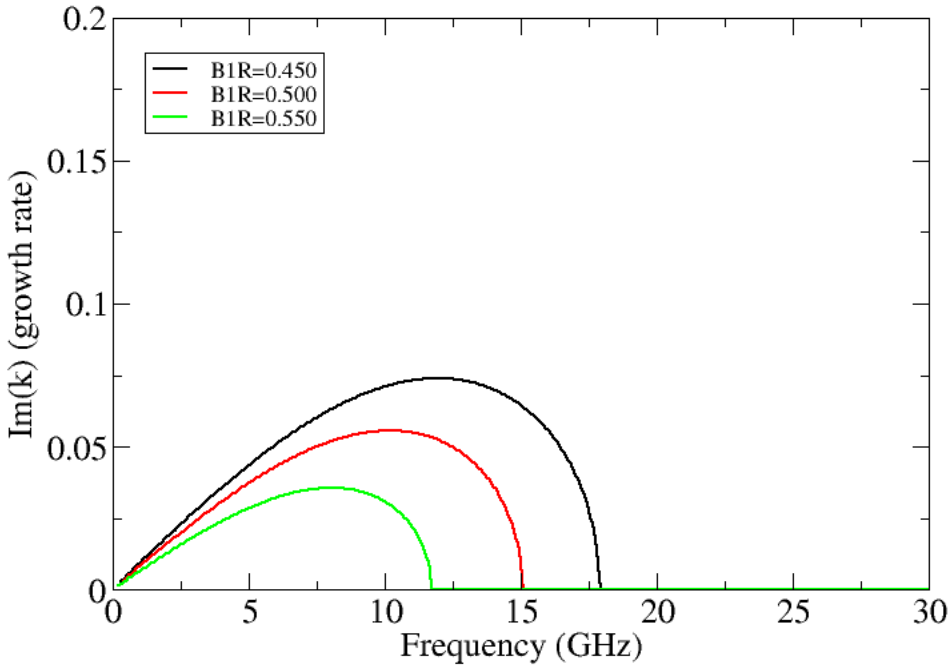

Figure C-3: Family Of Curves For Varying Beam Currents

Table C-3: Electron Beam Parameters

Design	I_{bi}	V_{bi}	R_{bi}	t_{bi}	I_{bo}	V_{bo}	R_{bo}	t_{bo}
Various beam 1 radii	360A	240kV	see plot	1mm	1200A	500kV	3mm	1mm

4.0 Theory Curves for Various Inner Beam Voltages

The theory curves in Figure C-4 illustrate the effect of varying the voltage of the low current, inner beam. The values B1V are in kV, other beam parameters are listed in Table C-4, and the beam tunnel was 0.95cm in radius. These designs were not tested via PIC simulation.

Table C-4: Electron Beam Parameters for Beam 1 Voltage Scan

Design	I_{bi}	V_{bi}	R_{bi}	t_{bi}	I_{bo}	V_{bo}	R_{bo}	t_{bo}
Various beam 1 voltages	360A	see plot	.2cm	1mm	1200A	550kV	0.3cm	1mm

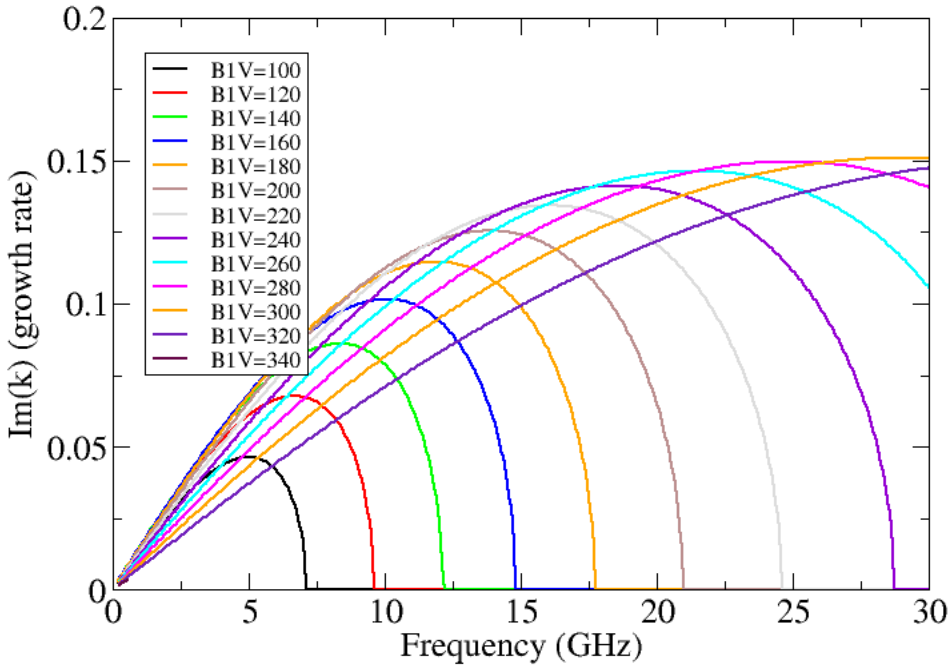

Figure C-4: Family Of Curves For Varying Inner Beam Voltages

Table C-5: Electron Beam Parameters for Beam 2 Voltage Scan

Design	I_{bi}	V_{bi}	R_{bi}	t_{bi}	I_{bo}	V_{bo}	R_{bo}	t_{bo}
Various beam 1 voltages	360A	240kV	.2cm	1mm	1200A	see plot	0.3cm	1mm

5.0 Theory Curves for Various Outer Beam Voltages

The theory curves in Figure C-5 illustrate the effect of varying the voltage of the high current, outer beam. The values B2V are in kV, other beam parameters are listed in Table C-5, and the beam tunnel was 0.95cm in radius. These designs were not tested via PIC simulation.

6.0 Growth Rate for Various Tube Radii

The theory curves in Figure C-6 illustrate the effect of varying the tube radius (TR). The values TR are in cm, other beam parameters are listed in Table C-6. Here it is seen that moving the conducting wall of the beam tunnel further from interaction with the beam enhances the growth rate of the instability. However, this also reduces the space charge limiting current, and thus the space charge limiting current and the beam tunnel radius are a pair of parameters that must be traded with each other to reach desired performance.

These designs were not tested via PIC simulation.

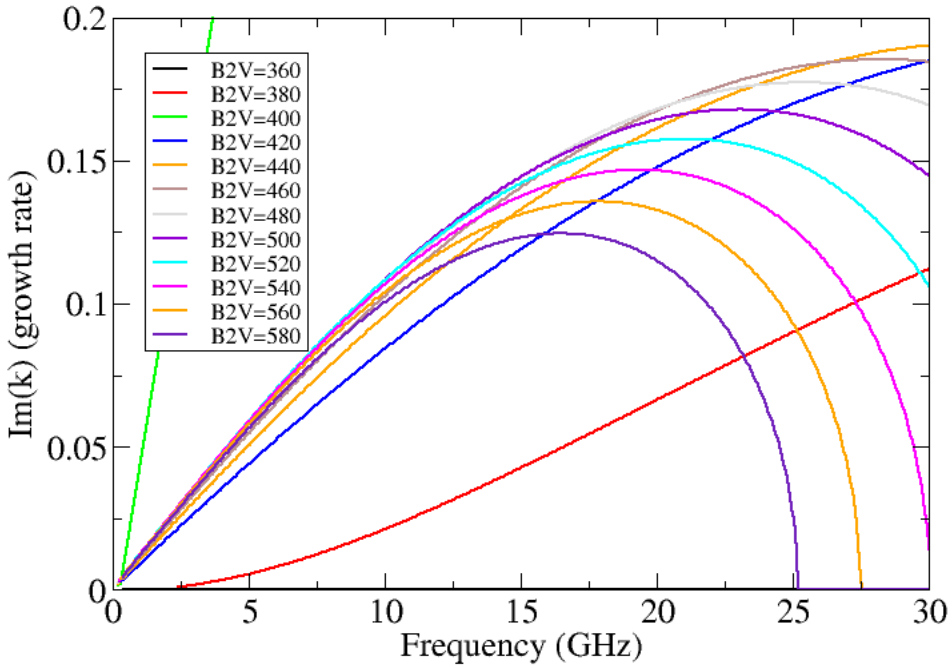

Figure C-5: Family Of Curves For Varying Outer Beam Voltages

Table C-6: Electron Beam Parameters For Tube Radius Scan

Design	I_{bi}	V_{bi}	R_{bi}	t_{bi}	I_{bo}	V_{bo}	R_{bo}	t_{bo}
Various tube radii	360A	240kV	0.2cm	1mm	1200A	550kV	0.3cm	1mm

7.0 11.4GHz Current Modulation Plots for Various Amplitudes of Input Signal

Figure C-7 shows the current modulation fraction for the 11.4GHz design discussed in Section 4.2, when an initial current modulation fraction of 0.0001 is imposed at 11.4GHz upon beam insertion at the left hand side of the simulation. Figures C-8, C-9, C-10, C-11 similarly show amplified current modulation as function of input current modulation for initial current modulation values of .0005, .005, .01, and .05. The lowest initial input is the most useful for calculating the optimum gain.

8.0 3D Simulations

In a search for unanticipated instabilities, such as diocotron instabilities, sausage instabilities, and other inherent 3D beam instabilites, some 3D simulations were performed in addition to all of the 2D simulations presented. An exhaustive search of all the parameters was not performed in 3D because of computational expense–instead, theory and 2D simulations were to be relied upon to narrow down the parameters of interest to relatively

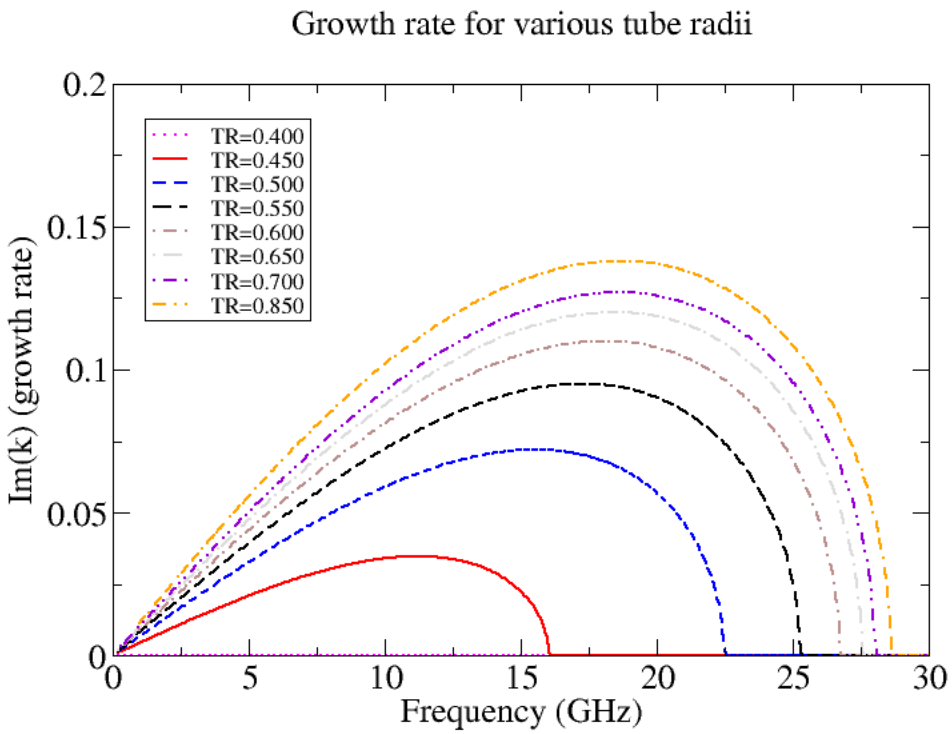

Figure C-6: Family Of Curves For Varying Beam Tunnel Radii

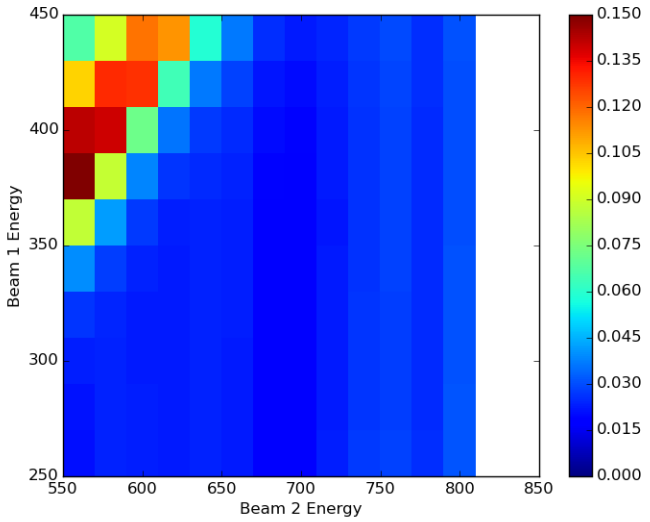

Figure C-7: 11.4GHz Current Modulation as a Function of Beam Energies, Initial Modulation Fraction 0.0001

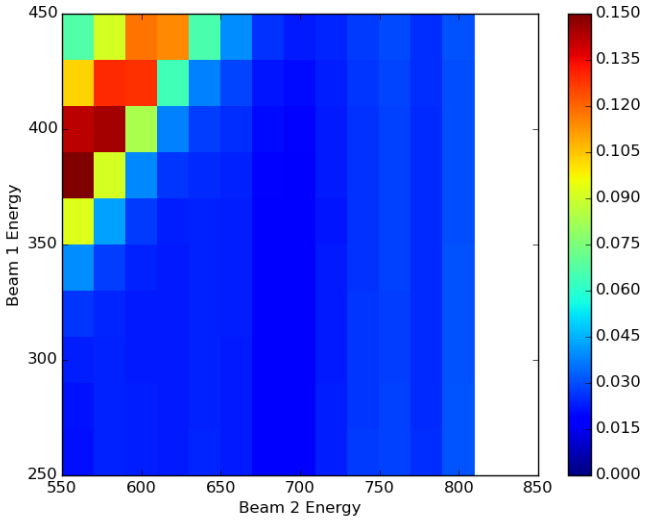

Figure C-8: 11.4GHz Current Modulation as a Function of Beam Energies, Initial Modulation Fraction 0.0005

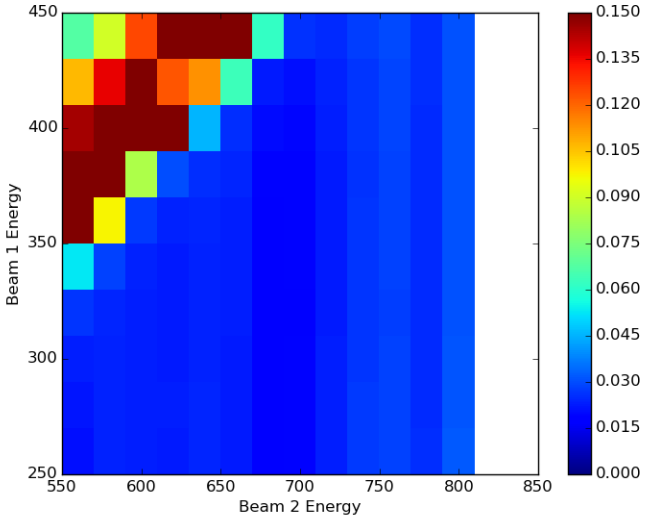

Figure C-9: 11.4GHz Current Modulation as a Function of Beam Energies, Initial Modulation Fraction 0.005

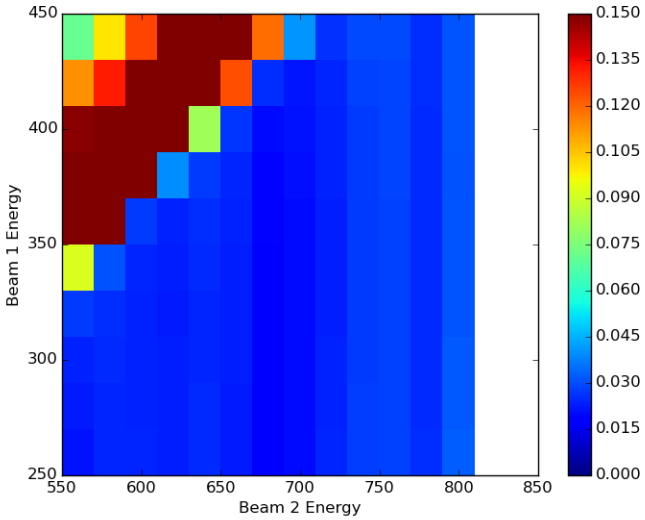

Figure C-10: 11.4GHz Current Modulation as a Function of Beam Energies, Initial Modulation Fraction 0.01

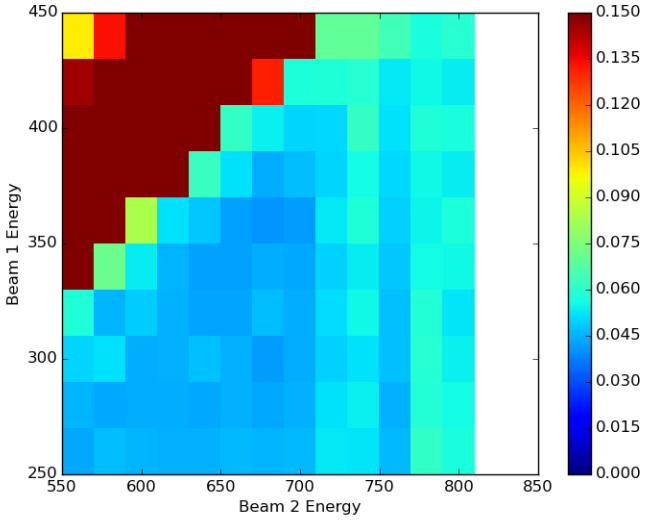

Figure C-11: 11.4GHz Current Modulation as a Function of Beam Energies, Initial Modulation Fraction 0.05

narrow ranges. When it became clear that physically producing the required beam parameters was not feasable with current technology, investigation into possible 3D instabilities was also halted. Still, a number of 3D simulations were performed using the baseline 3.375GHz design from Tables 1 and 2. Instead of injecting a signal, the simulations were allowed to amplify noise, and thus frequencies with the highest growth rate would be observed. Figure C-12 shows the non-DC current modulation amplitude at z=1.5m into the simulation. Note that this is somewhat differently presented than our typical current modulation plot, which shows the maximum modulation for every beam energy pair for all z values sampled in the simulation. This result is actually unfavorable because, ideally, when we are not inputting a signal, we do not want significant power output: producing output without input is oscillator behavior not amplifier behavior. This behavior was ultimately controlled via noise reduction techniques, such as removing the magnetic field dump, using more macroparticles injected per timestep, changing the beam extraction, and filtering.

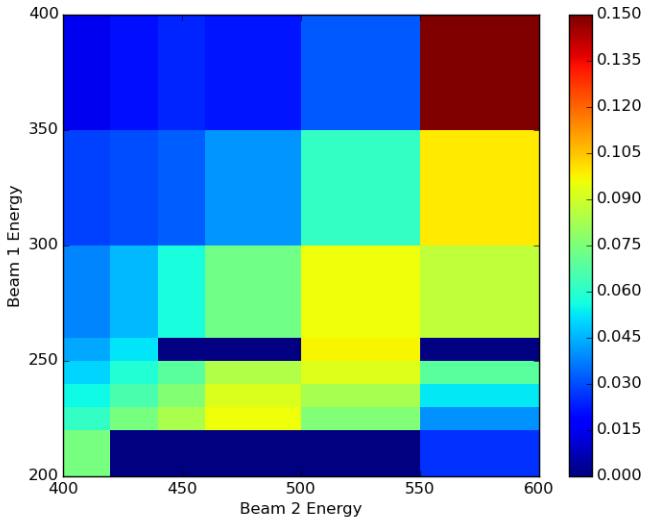

Figure C-12: 3GHz Current Modulation From 3D Simulation as a Function of Beam Energies at Z=1.5m, Amplifying Noise

LIST OF SYMBOLS, ABBREVIATIONS, AND ACRONYMS

2D	two dimensional
3D	three dimensional
A	Ampere
AFOSR	Air Force Office of Scientific Research
AFRL	Air Force Research Lab
AU	Arbitrary Units
B_0	Magnetic field
c	Speed of light
cm	centimeter
Dakota	Nonlinear optimization, sensitivity analysis, uncertainty quantification software
dB	decibel
dr	Numerical size in the radial direction
dz	Numerical mesh size in the z direction
DC	Direct current, meaning little to no time variation in current
EM	Electromagnetic
FDTD	Finite Difference Time Domain
GHz	gigahertz
GW	gigawatt
$\tilde{I}$	Current modulation
ICEPIC	Improved Concurrent Electromagnetic Particle In Cell
J_z	Current density in the z coordinate direction
kA	kilo ampere
keV	kilo electron volt
kV	kilo volt
kW	kilowatt
m	meter
mm	millimeter
MHz	megahertz
MW	megawatt
OOPIC	Object Oriented Particle In Cell
ns	nanosecond
PIC	Particle in Cell
PML	Perfectly Matched Layer
RF	Radio Frequency
RTKA	Relativistic Two-stream Klystron Amplifier
RTSA	Relativistic Two-Stream Amplifier
r-z	radius-z coordinate, meaning polar coordinates
θ	Theta, depending on context, an angle or a parameter for the Friedman filter
TE_{11}	Transverse Electric Electromagnetic Mode 1,1
TM_{01}	Transverse Magnetic Electromagnetic Mode 0, 1

TR	Tech Report or Tube Radius
TWT	Travelling Wave Tube
V	Volt
XOOPIC	X windows Object Oriented Particle in Cell

DISTRIBUTION LIST

DTIC/OCP
8725 John J. Kingman Rd, Suite 0944
Ft Belvoir, VA 22060-6218 1 cy

AFRL/RVIL
Kirtland AFB, NM 87117-5776 1 cy

Official Record Copy
AFRL/RDHE/Peter Mardahl 1 cy

This page intentionally left blank.